Received: 3 November 2023 | Revised: 29 December 2023 | Accepted: 4 January 2024

DOI: 10.1002/bte2.20230062

REVIEW

BATTERY ENERGY Open Access WILEY

Lithium dendrites in all-solid-state batteries: From formation to suppression

Huaihu Sun[1] | **Axel Celadon**[2] | **Sylvain G. Cloutier**[2] | **Kamal Al-Haddad**[2] | **Shuhui Sun**[1] | **Gaixia Zhang**[2]

[1]Institut National de la Recherche Scientifique (INRS), Centre Énergie Matériaux Télécommunications, Varennes, Québec, Canada

[2]Department of Electrical Engineering, École de Technologie Supérieure (ÉTS), Montréal, Québec, Canada

Correspondence
Shuhui Sun
Email: shuhui.sun@inrs.ca

Gaixia Zhang
Email: gaixia.zhang@etsmtl.ca

Funding information
Marcelle-Gauvreau Engineering Research Chair program; Natural Sciences and Engineering Research Council of Canada; Centre Québécois sur les Materiaux Fonctionnels (CQMF); Canada Foundation for Innovation (CFI); Institut National de la Recherche Scientifique (INRS); École de Technologie Supérieure (ÉTS)

Abstract

All-solid-state lithium (Li) metal batteries combine high power density with robust security, making them one of the strong competitors for the next generation of battery technology. By replacing the flammable and volatile electrolytes commonly found in traditional Li-ion batteries (LIBs) with noncombustible solid-state electrolytes (SSEs), we have the potential to fundamentally enhance safety measures. Concurrently, SSE would be capable of fitting high specific capacity (3860 mAh g^{-1}) metal Li and is expected to break through the upper limit of mass-energy density (350 Wh kg^{-1}) of existing LIBs system. Nevertheless, the growth of Li dendrites on the negative side or the nucleation of Li inside SSEs may give rise to battery short circuits, which is the primary factor limiting the application of Li metal. Recognizing this, the focus of this review is to provide a perspective for experimentalists and theorists who closely monitor various surface/interface and microstructure phenomena to understand Li dendrites. The strategies to reveal the complicated deposition mechanism and to control the dendrite growth of metal Li in solid-state batteries, as well as the advanced characterization methods of metal Li, provide suggestions for the practical research of solid-state Li metal batteries.

KEYWORDS

all-solid-state Li metal batteries, control strategy, deposition mechanism, Li dendrites, solid-state electrolytes

1 | INTRODUCTION

In light of the rapid evolution of the social economy and the gradual depletion of traditional fossil fuels, the development of novel energy storage devices assumes paramount importance in the strategic adjustment of energy structures, the promotion of environmentally sustainable practices, and the enhancement of overall energy utilization. Representing a contemporary paradigm in energy storage, lithium (Li) metal solid-state battery (SSB) employing a solid-state electrolyte (SSE) in lieu of conventional liquid electrolytes emerge as a viable solution to the challenges hampering significant advancements in safety and energy density.[1,2] This

efficacy arises from two primary factors. First, SSBs leverage Li metal with a low oxidation–reduction potential (−3.04 V vs. standard hydrogen electrode) and a high theoretical specific capacity (3860 mAh g^{-1}) to replace traditional graphite anodes. This strategic substitution, coupled with the compatibility of high-voltage cathode materials, enables the achievement of elevated power and energy density.[3] Second, the safety of the battery has been fundamentally improved because of the adoption of nonflammable SSEs.[4] For instance, SSBs successfully navigate acupuncture experiments, an insurmountable challenge for their traditional liquid counterparts. Additionally, SSEs demonstrate a greater propensity to impede the penetration of Li dendrites and suppress side reactions between Li and electrolytes when compared to their liquid counterparts on a macroscopic scale. Consequently, the practical potential of a metal Li anode in SSBs surpasses that of liquid batteries.

Nevertheless, numerous challenges persist in the pursuit of developing high-performance SSEs suitable for commercialization, as depicted in Figure 1.[5] Two decades ago, Monroe and Newman theoretically proposed that hindering dendrite penetration could be achieved when the shear modulus of polymer solid electrolytes surpasses twice that of Li metal.[6] However, despite extensive studies demonstrating the mechanical strength of polymer solid electrolytes and inorganic SSEs, Li dendrites continue to breach the electrolyte, causing short circuits, particularly at high current densities. Simultaneously, there is no scientific consensus on why such a "soft" Li metal grows into a "hard" SSE due to the lack of statistical data related to high-quality controlled experiments. Presently, two prominent hypotheses posit that Li dendrites arise from (1) pre-existing mechanical defects in the electrolyte driven by mechanical fracture and (2) excessive electronic conductivity in the

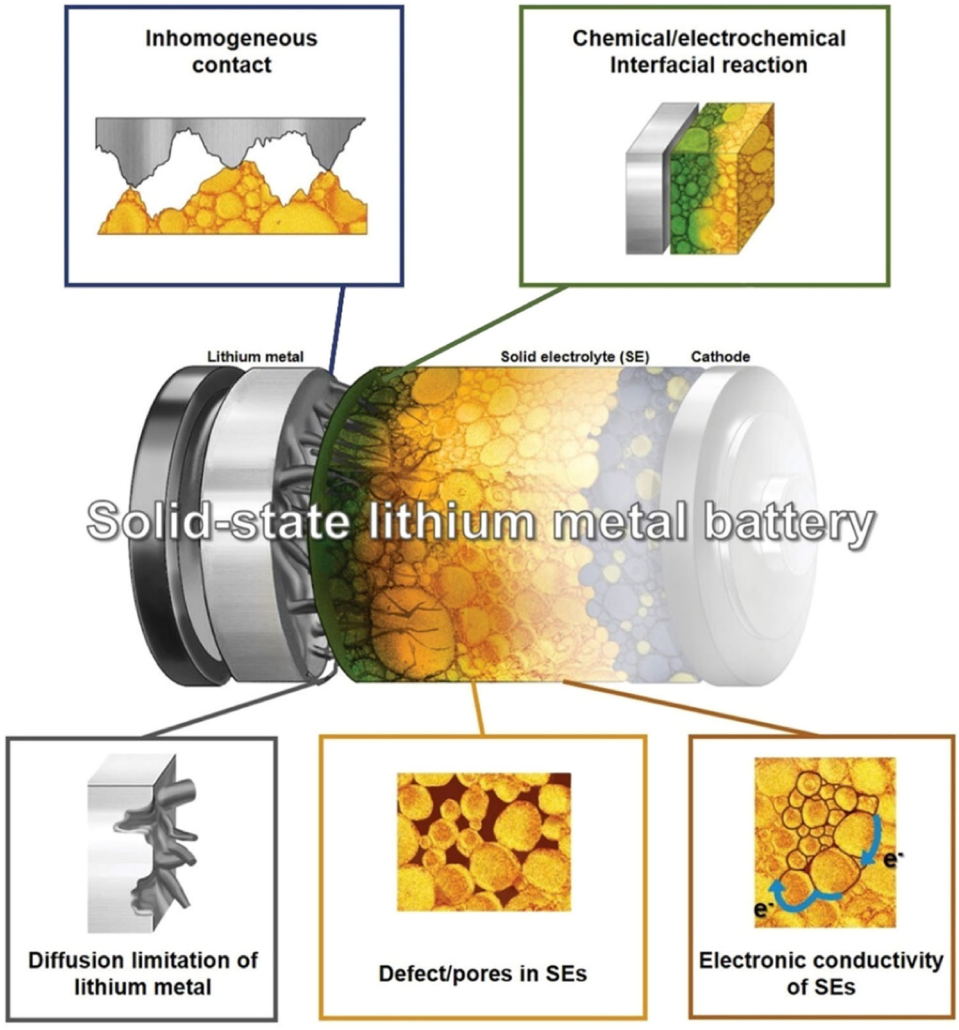

FIGURE 1 Schematic illustration of the main challenges faced in solid-state lithium metal battery reproduced with permission Yoon et al.[5] Copyright 2021, Wiley.

electrolyte propelled by electrochemical degradation of SSEs. Furthermore, substantial disparities in the transport behavior of Li ions in SSEs versus liquid electrolytes exist, and the deposition behavior of metallic Li at the interface of solid electrolyte phases varies across spatial and temporal scales.[7] Consequently, a more systematic and in-depth understanding of the growth mechanism of Li metals becomes imperative, incorporating perspectives from thermodynamics, kinetics, material stress, structural stability, and beyond.

To address the challenges associated with Li metal anodes, researchers have proffered a range of solutions falling under three categories: surface modification, composition regulation, and structural design. These encompass diverse strategies such as interface wetting solutions, hydrophilic modification layers, composite electrolytes, composite Li metal anodes, three-dimensional SSE structures, and three-dimensional anode designs.[8–16] Nevertheless, the complexity of anode interface properties and the diverse fundamental issues of solid-state lithium metal batteries (SSLMBs) with distinct electrolyte systems invariably necessitate twice the effort on account of devising effective solutions. In light of these considerations, this review centers on a systematic discussion classifying the deposition mechanism of metallic Li in mainstream SSEs. It delves into strategies for controlling Li metal deposition within the SSE, compiles characterization methods for assessing Li deposition behavior in SSBs, and briefly outlines anode-side design methodologies for industrialization. The aim is to offer guidance for the advancement of SSB technology.

2 | CHALLENGES ARISEN BY LI DENDRITES

In theory, SSLMBs embody the desirable properties of safety, high specific energy, and prolonged cycle life, fulfilling the expectations of researchers. However, numerous practical impediments emerge as SSLMBs find increased utilization. As illustrated in Figure 2, contrary to expectations, Li dendrites not only persist in their growth within SSE but can penetrate even the rigid ceramic SSE, resulting in short circuits in SSB.[17] Furthermore, despite achieving ionic conductivity levels comparable to liquid electrolytes, the current solid–solid contact between the anode and the electrolyte constrains ion transfer efficiency, potentially leading to electrolyte decomposition at the interface.[18] The stringent requirements imposed by solid–solid contact also pose challenges related to the volume expansion of electrode materials, where even slight changes can induce the cracking of rigid and brittle ceramic electrolyte sheets during cycling. Addressing these challenges necessitates a comprehensive understanding of interface chemistry, Li deposition behavior, and their intricate correlations.

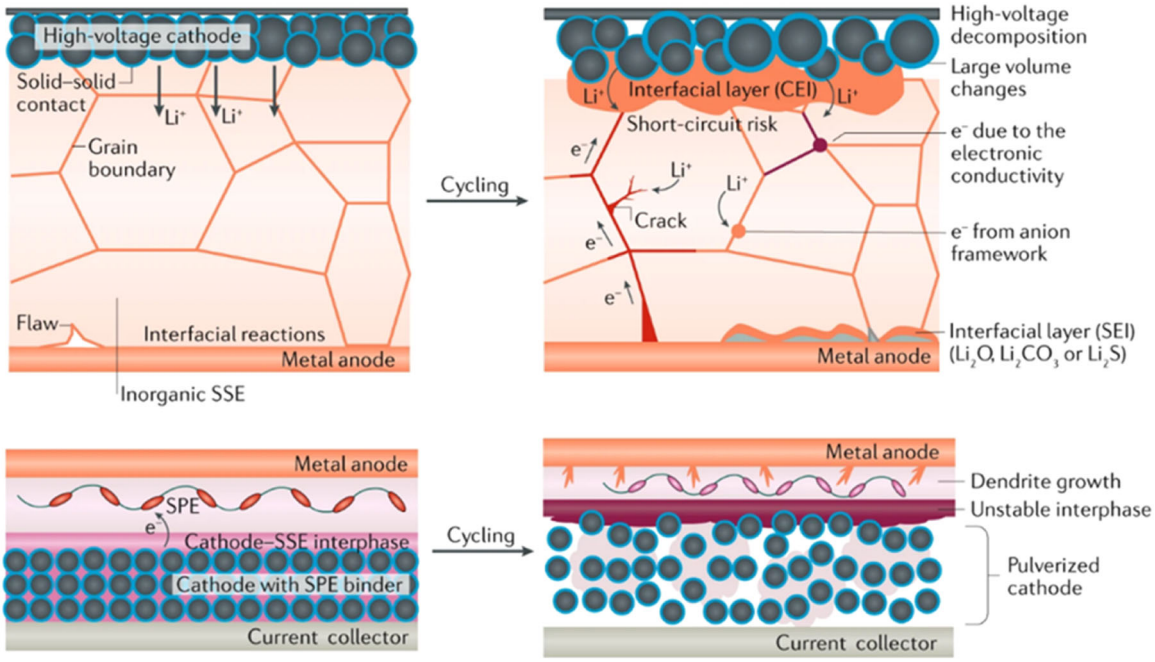

FIGURE 2 Common failure mechanisms originate from Li dendrites. Reproduced with permission Zhao et al.[17] Copyright 2020, Springer Nature.

2.1 | Li/SSE interface contact

Attaining precise electrode/electrolyte interface contact stands as a fundamental prerequisite for ensuring optimal battery performance. However, an imperfect interface contact is observed at the Li/SSE interface, giving rise to heightened interface impedance and hindering the efficient transport of Li^+ ions and electrochemical reactions involving metallic Li at the interface. Figure 3A delineates this issue into distinct categories, namely initial contact challenges and contact issues arising after cycling, corresponding to different phases of interface contact problems.

The primary challenge in initial contact arises from the contact mode at the solid–solid interface and the presence of impurities on both the metal Li and SSE. On one hand, the inherent contact between the rigid SSE and Li anode primarily involves solid–solid contact, often characterized by a point-to-point contact mode, limited contact area, and the presence of pores. Despite the high density of inorganic SSE, the surface remains notably rough due to the preparation process, complicating efforts to establish close contact with metal Li. Thin film SSBs, grown through physical vapor deposition, achieve improved interface contact and relatively stable cycle performance. However, their application scope is restricted by the low surface capacity of thin film batteries. Even with high-density inorganic SSE, the surface remains exceedingly rough, impeding intimate contact with metal Li. On the other hand, metal Li, with strong reducibility, tends to form impurities such as Li_2O and lithium carbonate (Li_2CO_3) on the surface during storage and transfer. This not only diminishes the actual contact area between Li and SSE but also hinders Li^+ conduction at the interface due to the low ionic conductivity of the impurities.[22,23] Current methodologies commonly involve heating and melting the low-melting-point metal Li (180°C). After heating, the original solid–solid contact transforms into solid–liquid contact, with the expectation of enhancing the uniformity and consistency of interface contact. However, molten Li often fails to wet SSE in experiments. Sakamoto et al. identified impurity Li_2CO_3 on the surface of $Li_7La_3Zr_2O_{12}$ (LLZO) as the main obstacle to interface wetting through density functional theory calculations, confirming the inherent wetting of Li and LLZO (Figure 3B).[20] Despite these findings, some researchers contend that impurities on the Li surface predominantly affect interface wetting (Figure 3C,D).[21]

2.2 | Uncontrollable Li dendrite growth

The uncontrolled proliferation of Li dendrites poses the most formidable challenge in liquid Li metal batteries.

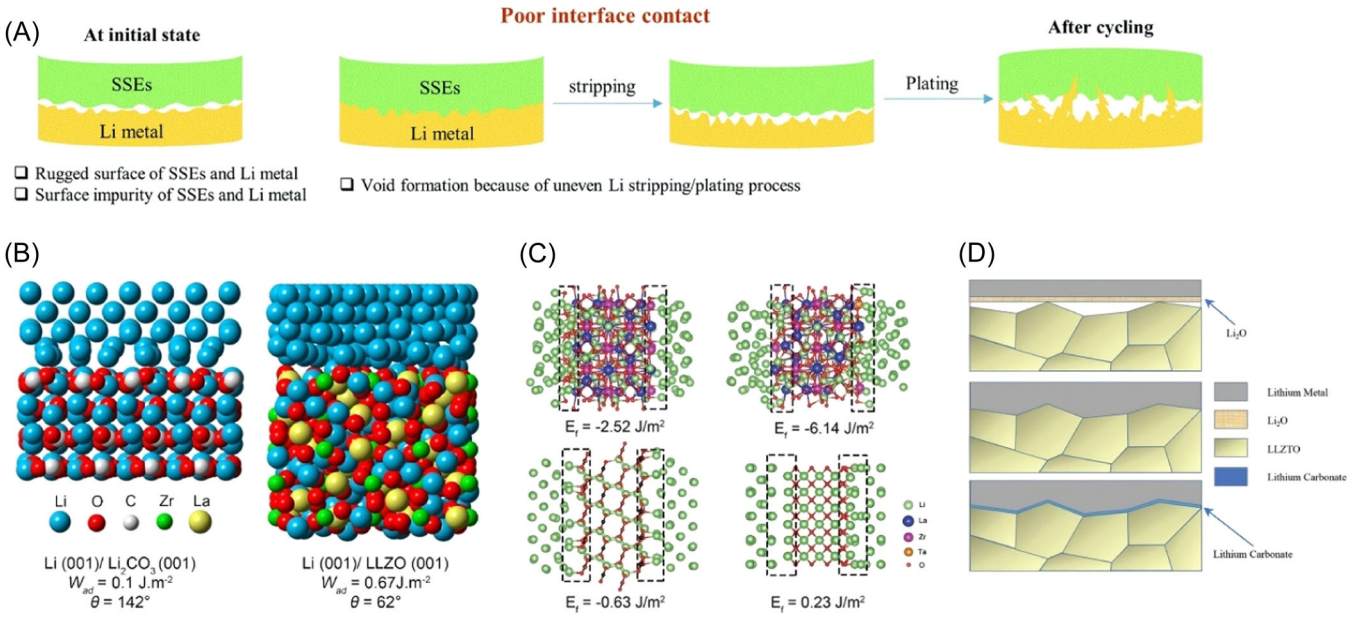

FIGURE 3 (A) Schematic representation of the interfacial contact issue between Li/SSE. Reproduced with permission Sun et al.[19] Copyright 2020, Royal Society of Chemistry. (B) Calculation results for the work of adhesion (W_{ad}), contact angle (θ), and atomic structure for the Li-Li_2CO_3 and Li-LLZO interfaces. Reproduced with permission Sharafi et al.[20] Copyright 2020, American Chemical Society. (C) Optimized interface structures of Ta-doped LLZO (LLZT)/Li, LLZT/Li, Li_2CO_3/Li, and Li_2O/Li, along with corresponding interface formation energies. (D) Illustration depicting distinct wetting behaviors of garnet surfaces with molten Li. (C and D) Reproduced with permission Zheng et al.[21] Copyright 2019, Wiley.

While the integration of SSEs can to some extent mitigate dendrite growth, it remains inevitable, especially under high current density. The emergence of dendrites directly leads to micro short circuits or complete battery short circuits, resulting in battery failure. The underlying cause of dendritic growth is the uneven deposition of Li metal. Research has substantiated that Li metal initially deposits at grain boundaries and subsequently accumulates on the surface of electrolyte particles.[24] This phenomenon gives rise to localized Li metal deposition, generating ultrahigh stress exceeding 150 GPa.[25] This stress induces the breakage of the electrolyte sheet's surface, exacerbating the uneven deposition, thereby creating a vicious cycle that ultimately leads to the penetration of Li dendrites through the electrolyte sheet. F. Aguesse et al. disassembled $LiFePO_4$|Ga-LLZO|Li batteries cycled 20 times at room temperature, revealing visible Li clusters (depicted as black substances) on the surface of LLZO, suggesting a potential pathway for metal Li infiltration (Figure 4A,B).[26] Another manifestation of uneven deposition is the formation of numerous fine pores in Li metals, excluding Li dendrites. Over cycling, these pores gradually increase, leading to interface degradation. Ren et al. conducted electrochemical cycling of Li on both sides of LLZO-type electrolytes at high current density, followed by dismantling the battery and immersing it in alcohol to corrode the Li metal while retaining the electrolyte portion. As shown in Figure 4C, scanning electron microscope (SEM) images reveal the formation of a channel composed of abundant voids due to the deposition of Li metal in LLZO, serving as the culprit for electrolyte short circuit and the gradual increase in interface impedance.[27] Presently, there are relatively few studies on this issue, primarily for two reasons: first, SSBs typically exert certain pressure during operation, compacting Li metal and reducing the impact of holes; second, some batteries operate at high temperatures, and the Li metal is relatively soft, making it challenging to create large pores.

2.3 | Interfacial volume effect

The interface volume effect is another critical aspect of the Li anode in SSBs. In traditional Li-ion batteries, the volume expansion of active substances during cycling is a significant factor hindering battery performance, especially for Si, Sn, and Al anodes based on conversion/alloying reactions, where volume expansion can reach up to 300%, 250%, and 100%, respectively.[28–31] The composite of Si with carbonaceous materials has been considered an effective strategy to stabilize electrodes by absorbing the stress generated by volume expansions, such as Si NP-carbon-graphene (Si@C-rGO) composite with the sandwich structure achieve a volume variation of less than 10% after Li-ion insertion.[32] On the other hand, commercial graphite electrodes undergo only about 13.2% volume change per cycle after intercalation of Li ions/alloying.[33] Furthermore, cathode materials such as $Li_4Ti_5O_{12}$ with a stable structure exhibit unique "zero strain" characteristics during cycling.[34–36] However, for frameless materials like metal Li, the relative size change after cycling may be infinite once Li dendrites grow on its surface.[37] The

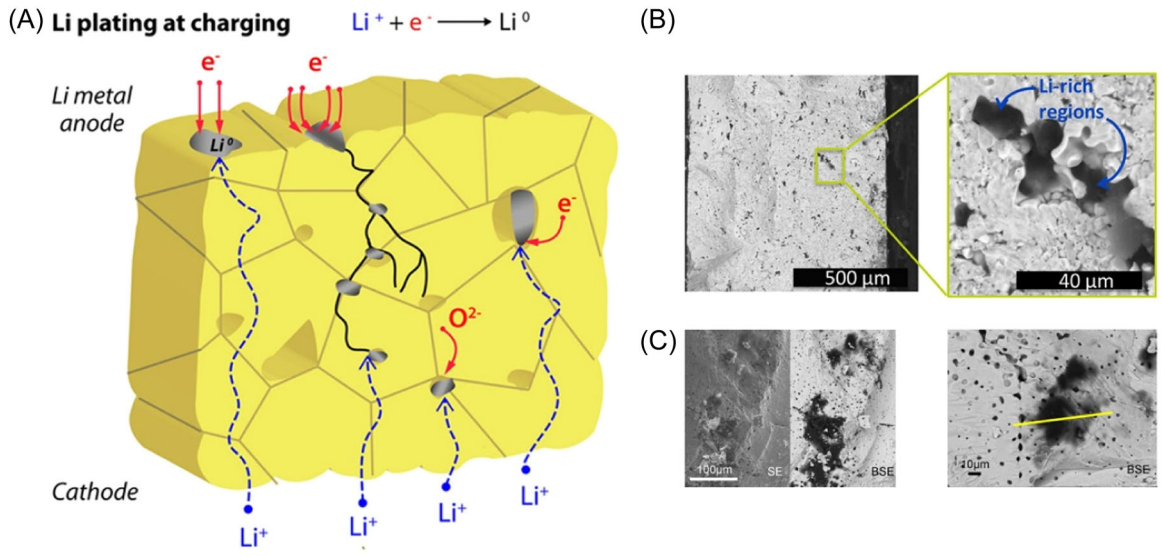

FIGURE 4 (A) Schematic representation of the ideal Li deposition path and potential dendrite growth path. (B) Cross-sectional scanning electron microscope (SEM) image of a fractured pellet obtained by solid-state electrolyte. (C) Magnified SEM images of the local region. (A–C) Reproduced with permission Aguesse et al.[26] Copyright 2017, American Chemical Society.

deposition/stripping process of metallic Li at the Li/SSE interface involves significant volume changes and periodic fluctuations with cycling. The inelastic inorganic SSE will quickly lose compact physical contact at the interface after deep cycling. Batteries experiencing this volume effect during cycling may undergo measurable changes in thickness or even structural separation, significantly damaging the long-term cycling stability of SSLMBs.[38,39] For example, Zaghib et al. observed dramatic periodic fluctuations in the thickness of the Li anode during the electroplating/stripping of Li in SSLMBs, ranging from a reduction to 33 μm after the initial discharge to an increase of about 42 μm during the charging process.[39] The Li deposition layer exhibits a relatively loose structure after such long-term cyclic changes, leading to the deterioration of interface contact, increased interface impedance, and heightened battery polarization. The interface volume effect also induces changes in interface stress. Janek et al. characterized the volume effect inside the battery by in-situ monitoring the pressure change of SSBs.[40] Figure 5A,B shows that only a small negative pressure was observed when $Li_4Ti_5O_{12}$ was adopted as the anode. In contrast, the stress of the entire battery became positive, and the pressure value exhibited periodic changes between 10 and 20 times when Li metal was employed as the anode, intuitively demonstrating the drastic volume change in the negative electrode interface cycle. Moreover, the growth of dendrites also induces serious volume effects, as illustrated in Figure 5C,D, where the irregular infiltration of Li metal in Al-doped LLZO ceramics accelerates the final rupture of the ceramic electrolyte.[41]

3 | ORIGIN OF UNCONTROLLED LI DENDRITES

Generally speaking, the genesis of Li dendrites in SSEs can be attributed to mechanical instability, represented by mechanical fracture in the electrolyte, and electrochemical instability, depicted by the electrochemical degradation of the electrolyte. This can be further delineated into the following situations: (1) growth along grain boundaries and voids in SSEs, where the intrinsic reason for dendrite formation is the low Li-ion diffusion rate at grain boundaries; (2) the growth of defects along

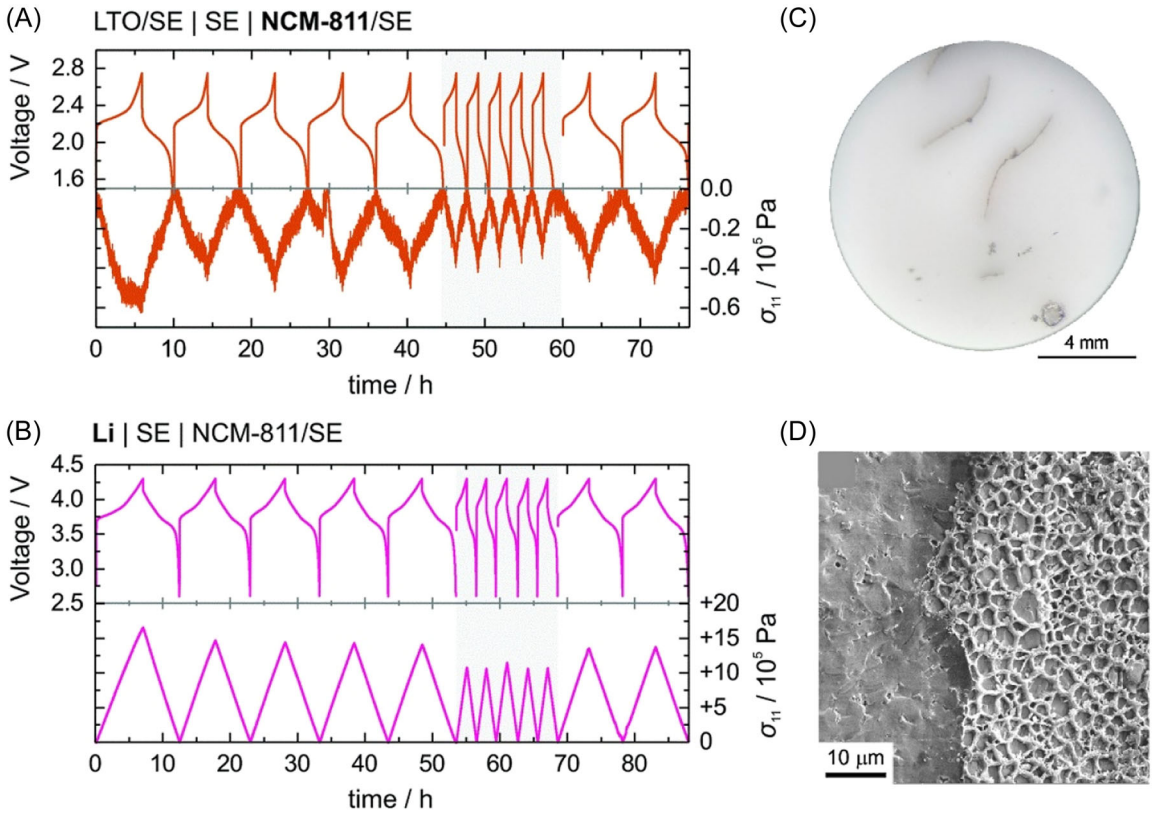

FIGURE 5 (A and B) Stress fluctuations induced by galvanostatic cycling for /solid-state electrolyte (SSE) | SSE | NCM811/SE solid-state cell and a Li|SSE | NCM811/SE solid-state cell. Reproduced with permission Koerver et al.[40] Copyright 2018, Royal Society of Chemistry. (C and D) Digital photographs and scanning electron microscope images illustrating the cycled LLZO pellet. Reproduced with permission Cheng et al.[41] Copyright 2017, Elsevier.

the surface or inside SSE is believed to induce dendrite formation, and the stress generated by dendrite growth further amplifies cracks, promoting the expansion of Li dendrites; (3) the uneven Li coating caused by insufficient interface contact between Li and SSE is also considered a source of dendrite formation; (4) the high electronic conductivity of SSEs accelerates the formation and growth of Li dendrites. Nowadays, researchers have proposed several models (Table 1) for the formation and early growth of Li dendrites, including the space charge model, Monroe–Newman model, heterogeneous nucleation model, deposition and dissolution model, and stress-driven model.[42]

3.1 | Space-charge model

Chazalviel et al. investigated the impact of local electric field enhancement resulting from the depletion of anions on the anode side on dendritic growth.[43] The model considers the growth of metal electrodeposition in a two-dimensional geometry starting from a linear cathode and conceives a thin rectangular battery while neglecting convection in the electrolyte. In this model, the depletion of anions and the accumulation of Li^+ ions near the anode create concentrated space charges and strong electric fields, thereby inducing the growth of "dendritic" Li. To validate this theory, simulations were conducted on ion concentration and electrostatic potential in the electrolyte. The growth of dendriform Li metal was triggered when the consumption rate (reaction rate) of Li^+ exceeded the supply rate (mobility of Li^+), considering both anions and cations. The ion concentration gradient in the battery follows Equation (1), and the gradient distribution is illustrated in Figure 6A.

$$\frac{\delta C}{\delta x} = \frac{J\mu_A}{FD(\mu_A + \mu_{Li^+})}, \tag{1}$$

where J is the current density, μ_A is anion migration number, μ_{Li^+} is Li^+ migration number, and D is the bipolar diffusion coefficient.

Considering the influence of the electric field, the voltage gradient in the battery follows the curve shown in Figure 6B, where area I is the quasi-neutral area and area II is the space charge area. Obviously, there is still a certain amount of space charge on the anode surface, generating a large local electric field that induces the formation of dendrites. The growth rate of dendrites follows the equation.

$$v_a = -\mu_a E_0, \tag{2}$$

where μ_a is the mobility of anions in the electrolyte and E_0 is the electric field strength in the neutral region of the electrolyte.

3.2 | Sand's model

In the electroplating process of Li metal batteries, mass transfer plays a crucial role. Solvated Li ions initially migrate under the influence of the electric field force, adsorb on the outer side of the electrode double layer, undergo desolvation, and come close to the surface of the Li metal. They are then reduced and adsorbed, becoming lattice atoms of Li.[47] Irregularities in the mass transfer process may eventually result in uneven metal deposition. In 1901, Sand et al. reported that during metal electrodeposition in a mixed solution of $CuSO_4/H_2SO_4$, cations and anions moved in opposite directions. Cations gathered near the anode and were continuously consumed. This led to changes in the salt concentration on the surface of the negative electrode, further causing copper dendrification.[48] The deposition mode would shift from stable deposition to self-amplifying dendritic growth when the salt concentration on the anode surface reached zero. The critical time for the appearance of dendrites, also known as Sand's time, is as follows.

$$\tau = \pi D\left(\frac{C_0 eZ_c}{2J}\right)^2\left(\frac{\mu_A + \mu_C}{\mu_A}\right)^2. \tag{3}$$

In the equation, D represents the bipolar diffusion constant, μ_C and μ_A represents the migration number of cations and anions, e represents the elemental charge, J represents the current density, Z_c represents the number

TABLE 1 Theoretical models for dendrite formation and corresponding strategies.

Models	Mechanisms	Strategies	References
Space-charge model	Ion diffusion and depletion	Dendrite suppression	[43]
Monroe–Newman model	Morphology and evolution of dendrites	Reduce the current density at the tip	[44]
Stress relaxation model	Residual stress release	Dendrite elimination	[45]
Deposition and dissolution model	Surface tension regulation	Dendrite suppression	[46]

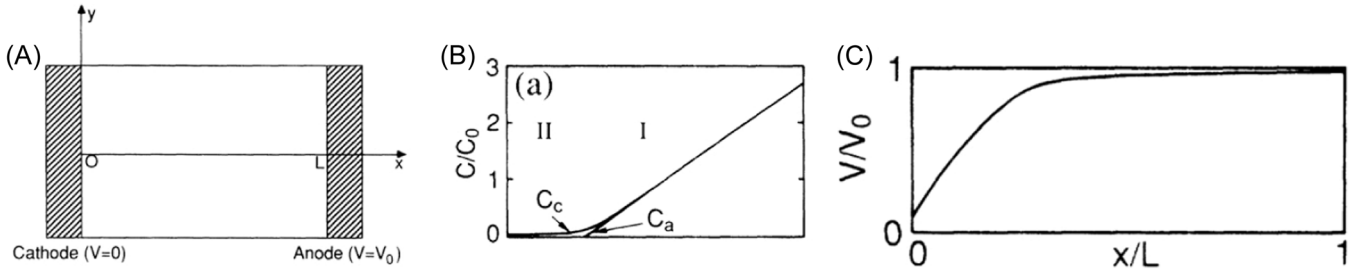

FIGURE 6 (A) Schematic illustration of symmetrical battery setting based on simulation. (B) Schematic representation of anion and cation concentration distribution. (C) Schematic diagram of voltage distribution. (A–C) Reproduced with permission Chazalviel.[43] Copyright 1990, American Physical Society.

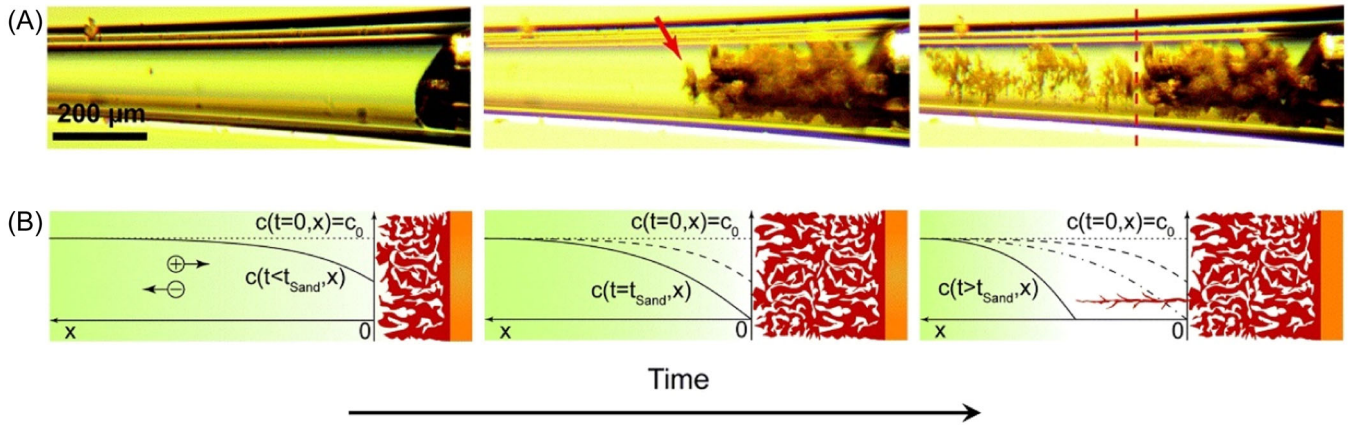

FIGURE 7 (A) In situ measurements of Li electrodeposition in a glass capillary containing an electrolyte solution. (B) Dendritic growth process resulting from cation depletion. (A and B) Reproduced with permission Bai et al.[55] Copyright 2016, Royal Society of Chemistry.

of charges carried, and C_0 represents the initial cation concentration. The illustration diagram of the growth process of dendritic Li caused by the depletion of cations on the electrode surface is shown in Figure 7A,B. It was observed in a glass capillary tube containing a Li||Li symmetric cell that when a constant current was applied, mossy Li began to precipitate and the salt concentration near the surface began to decrease while the voltage gradually increased.[49] Following approximately 40 min of polarization, the voltage initiates divergence as salts on the anode surface are depleted, leading to the abrupt emergence of slender dendrites exhibiting a distinct tip growth pattern.[50] This results in the formation of stagnant mossy Li. The two contrasting morphologies of Li deposition observed in situ within glass capillaries signify two distinct mechanisms: the transition from reaction-limited to transport-limited growth during voltage spikes. In the early stages of electrodeposition, mossy Li, primarily growing from its roots, appears as microscopic scale whiskers, with Li tips undergoing minimal shape changes upon displacement.[51–53] This random surface growth characterizes reaction-limited deposition. Due to the development of an insulating solid electrolyte interface (SEI) on individual Li whiskers, mossy Li remains incapable of transforming into a uniform metallic film through the ripening process, even under mechanical pressure. During voltage spikes, sparse Li dendrites experience explosive growth from their tips, forming a fractal morphology marked by diffusion-limited aggregation.[54]

3.3 | Monroe–Newman's model

Monroe and Newman et al. delved into the impact of dendritic morphology and its evolution on ion concentration and electric field distribution.[6,56] Employing a singular "whisker" Li as the model (Figure 8A), they contested the theory of constant growth rate proposed by Chazalviel, asserting that its growth rate would also vary with time, in accordance with the following equation:

$$v_{tip} = \frac{J_n V}{F}, \quad (4)$$

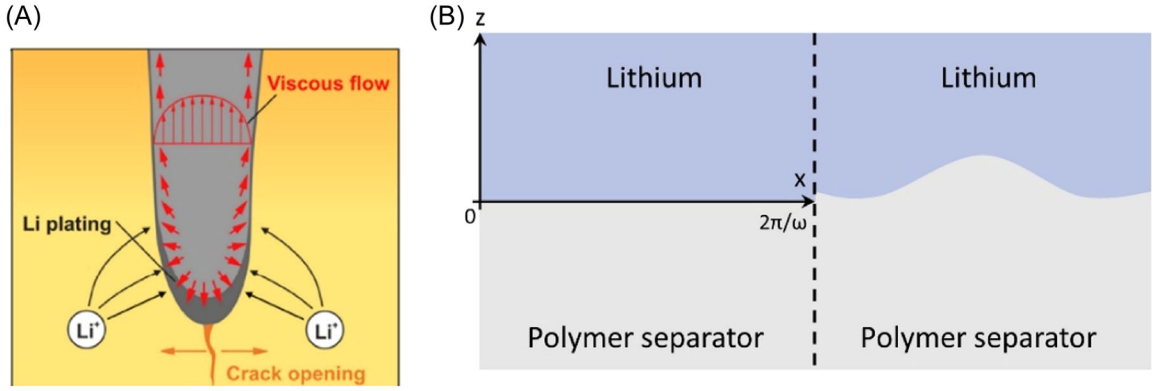

FIGURE 8 (A) Schematic diagram of the region near the dendrite tip. Reproduced with permission Krauskopf et al.[57] Copyright 2020, American Chemical Society. (B) Mechanical illustrating of solid electrolyte matrix with simplified Li filaments.

where v_{tip} is the growth rate of the tip, J_n is the current density of the tip, v is the Molar volume of Li metal, and F is the Faraday constant.

Moreover, the equation also suggests that reducing the current density at the tip can effectively impede dendritic growth. Further investigation delves into the impact of the deformation of polymer electrolyte with varying shear modulus on the growth of Li in a Li/polymer system. The ratio of the current (deformed) in the deformation area (right of Figure 8B) to the current (undeformed) in the deformation area (left of Figure 8B) yields the following equation, where α_a represents the number of anionic migrations, $\Delta\mu_{e-}$ is the potential change caused by local deformation, R is the standard Gas constant, A is the amplitude, $\cos(wx)$ is a periodic function. In Figure 8B, the x-axis corresponds to the horizontal displacement position of the constant undeformed material; the z-axis is the vertical displacement position of the constant undeformed material.

$$\frac{i_{\text{deformed}}}{i_{\text{undeformed}}} = \exp\left[\frac{(1-\alpha_a)\Delta\mu_{e-}}{RT}\right]. \tag{5}$$

$$\Delta\mu_{e-} \propto A\cos(wx). \tag{6}$$

$\Delta\mu$ always >0 in a low-modulus polymer system. At the Li tip, $A\cos(wx)$ always >0, and always <0 at peak-to-valley positions. The deposition rate of Li at the tip far outweighs other parts, resulting in an increase in the surface roughness of Li and rapid growth of dendrites.

$$\frac{\Delta\mu_{e-}}{A\cos(wx)} \equiv \Delta\mu > 0. \tag{7}$$

$$i_{\text{Lipeak}} > i_{\text{Livalley}}. \tag{8}$$

3.4 | Stress relaxation model

The electroplating process of Li will produce residual stress. Since the plated film usually has a relatively dense body and the defect volume is small, the stress is difficult to release inside the body, but will be concentrated on certain points of the electroplated film (such as grain boundaries and crystal impurities, Figure 9A), when the compressive stress exceeds the yield strength of Li metal, the local creep of Li will also cause more defect areas.[45,58,59] The bottom inorganic salt of the SEI is tightly attached to the Li metal surface, and some parts of the SEI layer containing pinholes or vacancies are most likely to undergo stress relaxation. The growth rate of whiskers is expressed by the following equation:

$$v_w = \frac{JV_{Li}}{\pi r^2}, \tag{9}$$

where V_{Li} is the molar volume of Li, r is the whisker radius, and J is the Li flux (mol s^{-1}), affected by compressive stress. Compressive stress can promote the diffusion of Li ions under compressive stress. If the growth rate of whiskers is higher than the uniform Li deposition rate ($v_p = \frac{JV_{Li}}{F}$, where J is the electroplating current density and F is Faraday's constant), Li will protrude in the form of whiskers.

When the compressive stress is large enough to destroy the interface layer, it will eventually lead to macroscopic dendritic Li growth.[60,61] In the initial stage of electroplating, Li overcomes the overpotential caused by nucleation on the substrate surface and is quickly covered by the SEI layer due to its high reactivity. As the electroplating process continues, stress simultaneously accumulates at the bottom of the coating. Once the stress reaches a threshold, the interface will be destroyed to release the pressure, and subsequent Li metal deposition

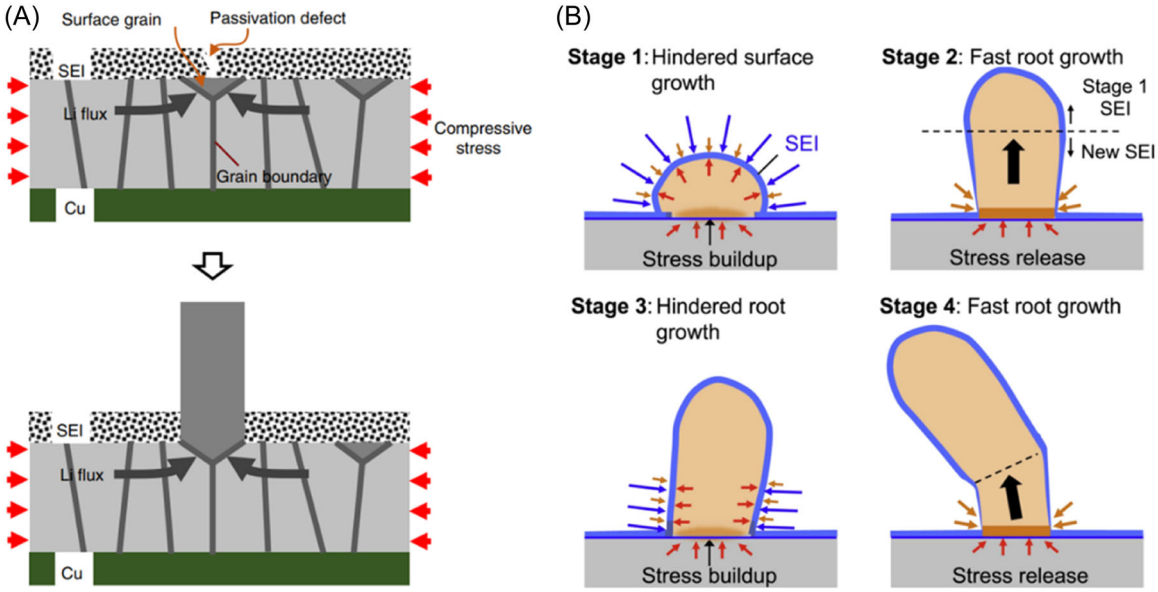

FIGURE 9 (A) Extrusion of lithium whiskers caused by surface defect sites. Reproduced with permission Wang et al.[45] Copyright 2018, Springer Nature. (B) Root Li growth caused by stress concentration. Reproduced with permission Kushima et al.[60] Copyright 2017, Elsevier.

will be triggered preferentially in fresh roots and evolve into Li whiskers due to free compressive stress and better electronic/ion conductivity. In the next Li plating cycle, stress will accumulate again and induce the next round of whisker growth (Figure 9B).[60] The uneven distribution of compressive stress inside the dendrite determines the uneven Li deposition on its surface, which will further lead to the plastic flow of Li atoms, release internal stress, and lead to tip bifurcation. Afterward, ion concentration and electric field induce preferential growth at the tips, ultimately giving rise to a dendritic macromorphology.

The focus of the aforementioned typical Li dendrite growth models varies: the space charge model contemplates the emergence of dendritic Li caused by the depletion of anions in the space charge region; the Monroe–Newman model attributes the growth rate of dendrites to the influence of the dynamic evolution of dendrites, analyzing the local current changes caused by the deformation of polymer systems; the stress relaxation model takes into account the residual stress inside the battery and offers a plausible explanation for the occurrence of whisker-like Li.

4 | STRATEGIES FOR INHIBITING DENDRITIC LI

Inspired by various irregular Li growth models, researchers have proposed numerous strategies to stabilize Li-ion current distribution and ensure uniform Li plating/stripping in SSLMB, thereby improving battery performance. From the perspective of battery structure composition, primary strategies encompass (1) Optimizing electrolyte composition; (2) Designing novel SSEs; (3) Constructing electronic insulation interface buffer layers; (4) Implementing surface modifications; (5) Modifying current collectors; (6) Introducing additional physical fields, and more.

4.1 | Optimization of electrolyte composition

LiI is presumed to be an effective additive for inhibiting the growth of Li dendrites. Suyama et al. simulated the dissolution/deposition behavior of Li in SSLMBs using the Li_3PS_4 (LPS)-LiI electrolyte system.[62] The electrochemical results indicate that the introduction of LiI enhances the dissolution/deposition ability of Li ions (Figure 10). Structural analysis reveals that the addition of LiI inhibits the reduction of electrolytes and maintains better interface contact even after a prolonged cycle time. In summary, the introduction of LiI mitigates the extent of the reduction reaction between SSEs and Li metal. Similarly, Han et al. also demonstrated that adding LiI to the electrolyte effectively inhibits the growth of Li dendrites in Li_2S-P_2S_5 glass phase electrolytes.[63] The high ion conductivity and electronic insulation of LiI promote the migration of Li ions at the interface, thereby preventing the growth of dendrites. The critical current density of the modified electrolyte significantly increased, reaching 3.9 mA cm^{-2} at 100°C. The Li symmetric cell steadily ran for 200 h at a surface current density of 1.5 mA cm^{-2}.

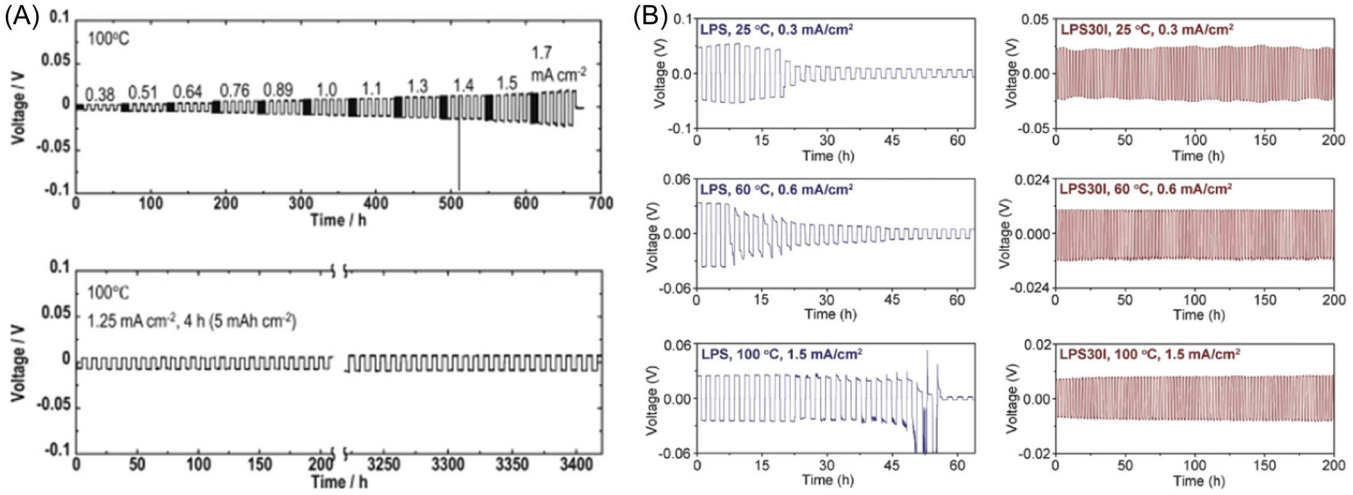

FIGURE 10 (A) Galvanostatic cycling tests of Li/54Li_3PS_4·46LiI/Li cells (where 54:46 is the molar percentage of the materials) with varied current density at 100°C. Reproduced with permission Suyama et al.[62] Copyright 2018, Elsevier. (B) Galvanostatic cycling of the Li/LPS/Li and Li/LPS30I/Li cells at constant current densities at 25°C, 60°C, and 100°C. Each charge and discharge cycle lasts 1 h. Reproduced with permission Han et al.[63] Copyright 2018, Wiley.

4.2 | Designing of novel SSEs

According to Brissot and Sand's model, anions and cations accumulate toward the positive and negative sides as they move freely in the electrolyte, creating a gradient in the concentration of anions and cations. This phenomenon results in the buildup of local space charges on the anode surface, forming a strong electric field and inducing the nucleation and growth of Li ions. In Equation (2), the time for the appearance of Li dendrites tends to infinity when the migration number of anions in the electrolyte approaches zero, implying an infinitely delayed appearance of Li dendrites. Following these design principles, single Li-ion conducting solid polymer electrolytes (SLIC-SPEs) have been developed to suppress Li dendrites. SLIC-SPEs involve polymers where anions covalently bond with polymers or inorganic frameworks or bind to anionic receptors in electrolytes and are immobilized, resulting in a low number of anionic migrations (Figure 11A,B).[64,65] As illustrated in Figure 11C, the symmetrical Li/SPE/Li cell exhibits a high transfer number of Li ions ($t_{Li}^+ = 0.97$) and favorable Li plating/stripping reversibility over about 1200 h. Research has demonstrated that immobilizing a small portion of anions achieves stable Li deposition in SSBs with a Young's modulus of only tens to hundreds of MPa, even at relatively high current densities.[66] Ye et al. sandwiched a less stable electrolyte between more stable electrolytes and produced an effect similar to an expansion screw by performing local decomposition in the less stable electrolyte layer, and the cracks caused by dendritic Li were eliminated via the generated decomposition.[67] Then the decomposition will produce an "anchoring" effect, hindering the growth of Li dendrites (Figure 11D). This multilayer structure design derived from electrochemical stability and instability allows the SSLMB equipped with NCM811 cathode to achieve a capacity retention rate of 92.8% after 1000 cycles at a charge/discharge rate of 1.5 C. Moreover, the design of multilayer composite solid electrolytes also follows this concept. The anion migration number in inorganic SSEs is approximately zero, so the Li-ion migration number of composite solid electrolytes can be greatly improved by designing a polymer-inorganic SSE-polymer sandwich structure. Guo's group found that the Li-ion migration number of polyacrylonitrile (PAN)-polyethylene oxide (PEO) double-layer SSE is only 0.41 (Figure 11F). However, the Li-ion migration number increased to 0.82 after coating PAN and PEO on both sides of $Li_{1.4}Al_{0.4}Ti_{1.6}(PO_4)_3$ (LATP), resulting in smaller long-cycle polarization of the battery and a more uniform and flat morphology of Li deposition, as shown in Figure 11G,H. It was observed that the hysteresis potential of the protected Li metal after 800 h of plating/stripping only increased by 22 mV when evaluating Li–Li symmetric batteries (Figure 11I). Compared with recent research in solid electrolytes, LATP ceramics exhibit interfacial stability toward Li anodes. In terms of the entire battery, the disparate-polymers protected ceramic electrolyte matched with NCM622 can maintain an excellent capacity of 89% after 120 cycles (135.6 mA h g^{-1}) at 0.5 C, with a coulombic efficiency (CE) exceeding 99.5% (Figure 11J). The group believes that the performance advance is due to LATP guiding the uniform distribution of ions, suppressing the formation of space charge layers at the SSE/Li anode interface, and thus controlling the generation of Li dendrites.[68]

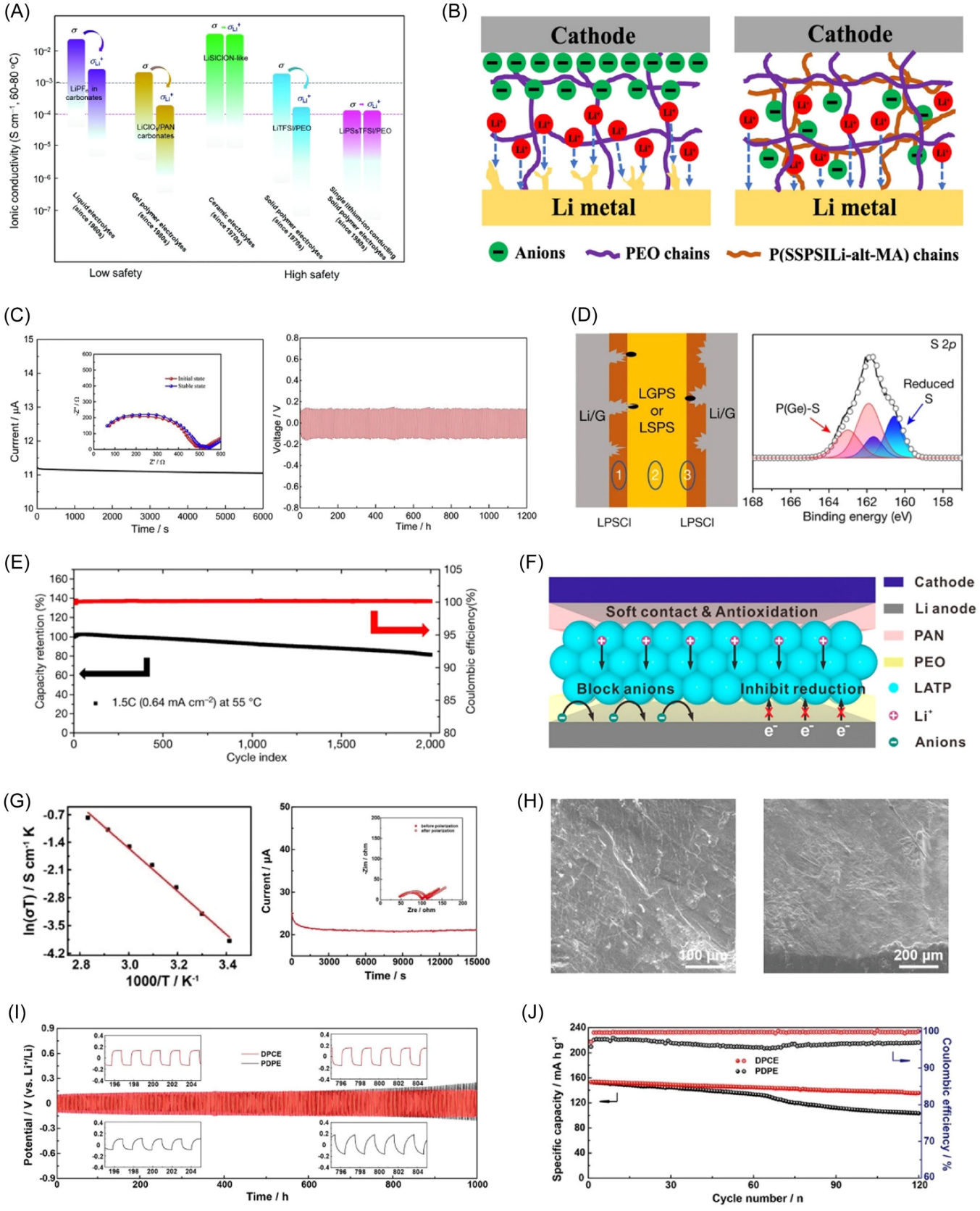

FIGURE 11 (See caption on next page).

4.3 | Construction of electronic insulation interface buffer layer

The establishment of a buffer layer between Li metal and SSE emerges as an effective path to suppress Li dendrites except for optimizing electrolyte composition. Table 2 comprehensively enumerates buffer layers prepared through diverse methods and their corresponding interface impedance with Li metal. Xu et al.'s investigation convincingly demonstrates that inducing a uniform LiF (or LiI) interface layer at the $Li/Li_7P_3S_{11}$ interface effectively inhibits the deluge of Li dendrites.[69] Employing methoxyperfluorobutane (HFE) and I_2 as precursors, a uniform reaction on the Li metal surface was conducted to create a LiF or LiI coating layer at 150°C. The coating process is schematically depicted in Figure 12A. LiF, with higher interface energy, demonstrates superior performance in suppressing Li dendrites compared to LiI coating. Significantly, even if the interface layer is penetrated by Li dendrites, the infiltrating HFE consumes fresh Li dendrites, forming a new SEI layer, as illustrated in Figure 12B. The results reveal an enhanced cycling performance of Li symmetric cells, achieving stable cycling beyond 200 cycles at current densities of 0.5 and 0.1 mA cm^{-2}. Assembled $LiNbO_3$@$LiCoO_2/Li_7P_3S_{11}$/LiF@Li SSLMBs exhibit a reversible discharge capacity of 118.9 mAh g^{-1} at a current density of 0.1 mA cm^{-2}. The reversible capacity is 96.8 mAh g^{-1} after 100 cycles, surpassing batteries equipped with pure metal Li. Wang et al. developed an aluminum-based organic-inorganic composite interlayer (alucone) between $Li_{10}SnP_2S_{12}$ and Li metal through the molecular layer deposition method (Figure 12C).[70] The results demonstrate that the artificial interface layer, serving as an SEI film, effectively blocks electron transfer at the $Li/Li_{10}SnP_2S_{12}$ interface, thereby completely inhibiting interface reactions and the growth of Li dendrites. Compared with a pure Li metal anode, all SSLMBs adopting modified Li metal anodes exhibit lower polarizability, higher capacity, and longer operational life (Figure 12D). Importantly, the organic–inorganic composite molecular layer exhibits superior flexibility compared to the inorganic coating layer, avoiding volume deformation.

4.4 | Surface modification

Surface modification is currently the most common approach for interface optimization, involving techniques such as surface chemical treatment and interface wetting.[8,9,89–91] Goodenough et al. successfully eliminated Li_2CO_3 from the electrolyte sheet's surface through carbon treatment, as depicted in the reaction formula: $2Li_2CO_3 + C \rightarrow 4Li^+ + 3CO_2 + 4e^-$ (Figure 13A).[8] Raman spectra of fresh LLZT revealed an uneven strong peak corresponding to Li_2CO_3 at 1090 cm^{-1}, whereas carbon-treated garnet (LLZT-C) showed no Li_2CO_3 (Figure 13B,C). Following Li_2CO_3 removal, the interface impedance of the symmetrical cell decreased from 5000 to 80 Ω. The symmetrical cell operated stably at 100 μA for over 500 h in the Li deposition/stripping experiment (Figure 13D). The author also assembled a half cell, with a $Li/Li_{6.4}La_3Zr_{1.4}Ta_{0.6}O_{12}$ (LLZTO)-C/$LiFeP_4$ cell impedance of approximately 300 Ω. The reversible discharge capacity reached 150 mAh g^{-1} after activation and stably cycled for more than 50 cycles, with a CE of about 97%. For Li/LLZTO-C/S batteries, their discharge capacity reached 1000 mAh g^{-1} and cycled over 60 cycles, with a CE approaching 100%. Huo et al. soaked LLZTO electrolyte tablets in 1 M hydrochloric acid and treated them with ultrasound for 30 s, successfully and quickly removing Li_2CO_3 attached to the surface.[92] As shown in Figure 13E, the surface of the

FIGURE 11 (A) Development roadmap for Li-ion conducting electrolytes in lithium-ion and rechargeable lithium batteries. Reproduced with permission Zhang et al.[64] Copyright 2017, Royal Society of Chemistry. (B) Diagrammatic representations that show how Li dendrites are suppressed in cells that have single Li-ion conducting solid polymer electrolytes (SLIC-SPEs). (C) Li symmetrical cell potentiostatic direct current polarization using a 20-weight percent SLIC-SPE membrane; the inset shows plots of the cell's alternating current impedance both before and after polarization. Voltage profiles for the Li symmetric cell with a 20 wt% SLIC-SPE membrane during galvanostatic discharge and charging. (B and C) Reproduced with permission Cao et al.[65] Copyright 2019, Elsevier. (D) The multilayer's various cross-sectional regions on the $Li_{5.5}PS_{4.5}Cl_{1.5}$ (LPSCl), $Li_{10}Ge_1P_2S_{12}$ (LGPS), and LPSCl-LGPS transition areas are illustrated along with X-ray photoelectron spectroscopy measurement of S 2p in the cross-section. (E) Retention of capacity and Coulombic inefficiency of solid-state battery with multilayer design cycled at 1.5 C with cut-off voltages set at 4.2 V. (D and E) Reproduced with permission Ye and Li.[67] Copyright 2021, Springer Nature. (F) Diagrammatic representations that the solid full battery with disparate-polymers protected ceramic electrolyte (DPCE). (G) Arrhenius linear fitting plots of the DPCE and the chronoamperometry curves and corresponding electrochemical impedance spectroscopy spectra before/after polarization for DPCE. (H) The top/side scanning electron microscope images of the Li-metal anode surface at the polyethylene oxide side. (I) Galvanostatic plating/stripping profiles of different electrolytes in the Li/Li symmetrical cells at 0.2 mA cm^{-2}. (J) Long cycling performance of solid-state lithium metal battery under 0.5 C. Reproduced with permission Liang et al.[68] Copyright 2019, American Chemical Society.

TABLE 2 Methods of suppressing the Li dendrites by promoting the SSE/Li interfacial contact and the corresponding interfacial performance.

Buffer layer	Experimental techniques	Interfacial impedance (Ω cm^{-2})	Cycling stability	Current density (mA cm^{-2})	References
Al_2O_3	ALD	1	Overpotential response at 22 mV for 90 h	0.2	[71]
ZnO	ALD	20	Polarization voltage ≈ 10 mV	0.1	[72]
Sn	Sputtering	46.6	Overpotential is only 0.07 V and remained for over 500 cycles	0.5	[73]
Au	Sputtering	380	Critical current density up to 0.8 mA cm^{-2} at 50°C	-	[74]
Au	Sputtering	450	Critical current density up to 200 μA cm^{-2}	-	[75]
Au	Sputtering	32	Short circuit occurs after cycling for 1.67 h	0.5	[76]
Nb	Sputtering	14	Stable operating within 50th cycle at 0.5 mA cm^{-2}	0.5	[76]
Si	Sputtering	5	Negligible polarization during the cycles for 120 h at 0.5 mA cm^{-2}	0.5	[76]
Mg	Sputtering	70	Polarization voltage ≈ 40 mV	0.1	[77]
Cu	Sputtering	29	Stable operating after 826th cycle	0.2	[78]
TO (indium tin oxide)	Sputtering	32	Without any fading of full batteries after 100th cycle at 0.2 C	-	[79]
Garnet-polymer (LLZO + PEO + $LiClO_4$)	Coating	413	No polarization of symmetrical cells after 140 h	0.06	[80]
MoS_2	Coating	14	Polarization voltage ≈ 8 mV	0.2	[81]
Liquid Metal Ga	Coating	5	130 mAh g^{-1} up to 440 cycles under 60°C	0.15	[82]
$Zn(NO_3)_2$	Dropping	-	No polarization of symmetrical cells after 2000th cycle	2	[83]
ZnO_2	Dropping	10	Polarization voltage < 100 mV	0.2	[84]
Graphite	Draw by hand	105	No failure of full batteries after 100th cycle at 0.5 C	-	[14]
S	High-pressure atomizer	160	No failure of symmetrical cells after 1100th cycle	0.2	[85]
Ti-doping LLZO	Pellet	-	No failure of symmetrical cells after 300th cycle	0.15	[86]

TABLE 2 (Continued)

Buffer layer	Experimental techniques	Interfacial impedance (Ω cm^{-2})	Cycling stability	Current density (mA cm^{-2})	References
Ge	Depositing	115	140 mAh g^{-1} up to 100 cycles with CE $\approx$ 100% at 5 C	-	[87]
Si	PECVD	127	No failure of symmetrical cells after 225th cycle	0.1	[88]

Abbreviations: ALD, atomic layer deposition; LLZO, Li7La3Zr2O12; PECVD, plasma-enhanced chemical vapor deposition; PEO, polyethylene oxide; SSE, solid-state electrolyte.

electrolyte sheet was covered with a thick layer of Li_2CO_3 before treatment, and the LLZTO particles below could not be observed at all. After treatment, the LLZTO particles had clear boundaries and a smooth surface, indicating that acid treatment effectively removed Li_2CO_3 (Figure 13F). A porous layer appeared on the surface when the processing time exceeded 5 min, so the processing time should not be too long. The interface impedance of the symmetrical cell decreased from 94 to 26 Ω cm^2 and remained stable for over 700 h at a current density of 0.2 mA cm^{-2} (Figure 13G). Wu et al. prepared electrolyte sheets without Li_2CO_3 by controlling sintering and storage conditions, and batteries assembled with them also achieved outstanding performance. Therefore, removing Li_2CO_3 through surface chemical treatment will effectively enhance battery performance.[89]

Liquids possess exceptional fluidity and elasticity, some of which were widely employed as interface wetting liquids in early SSLMB research. Two main types include traditional organic liquid electrolyte (OLE) systems and functional electrolyte-like systems. Introducing a small amount of traditional OLEs with high ionic conductivity (typically above 10^{-2} S cm^{-1}) effectively improves the interface, promoting ion conduction. However, precise control of the electrolyte amount is crucial due to its inherent flammability. Lu et al. wetted the LLZO-Li metal interface by dropwise addition of 10 μL cm^{-2} triethylene glycol dimethacrylate electrolyte containing 1 M LiTFSI. Three Li symmetric cell modes were designed, as depicted in Figure 14A–D: a mixed solid-state mode with electrolyte on both sides, a semisolid-state mode with electrolyte on one side, and an all-solid-state mode with no liquid.[93] Comparative analysis revealed that cells in semisolid and mixed solid-state modes exhibited stable cycling performance, even at high current densities of 1.5 mA cm^{-2}, while all-SSBs rapidly experienced short-circuit phenomena at 0.1 mA cm^{-2}. The analysis suggests that organic electrolytes guide the uniform conduction of Li^+ at the liquid–solid interface, inhibiting Li dendrite growth. Wang et al. found that the optimal addition amount was 2 μL cm^{-2}, and excess electrolyte provided no further contribution to battery performance (Figure 14E,F). Huo et al. also achieved favorable electrochemical performance by adding only 1.8 μL cm^{-2} ionic liquids at the interface between PEO/LLZTO composite electrolyte and the electrode.[94]

Due to the flammable and volatile nature of OLEs and their potential for side reactions with electrodes, efforts have been made to develop functional electrolyte-like systems. One type is to employ additives to protect the electrode/electrolyte and control the occurrence of side reactions. In fact, SSEs and OLEs are incapable of

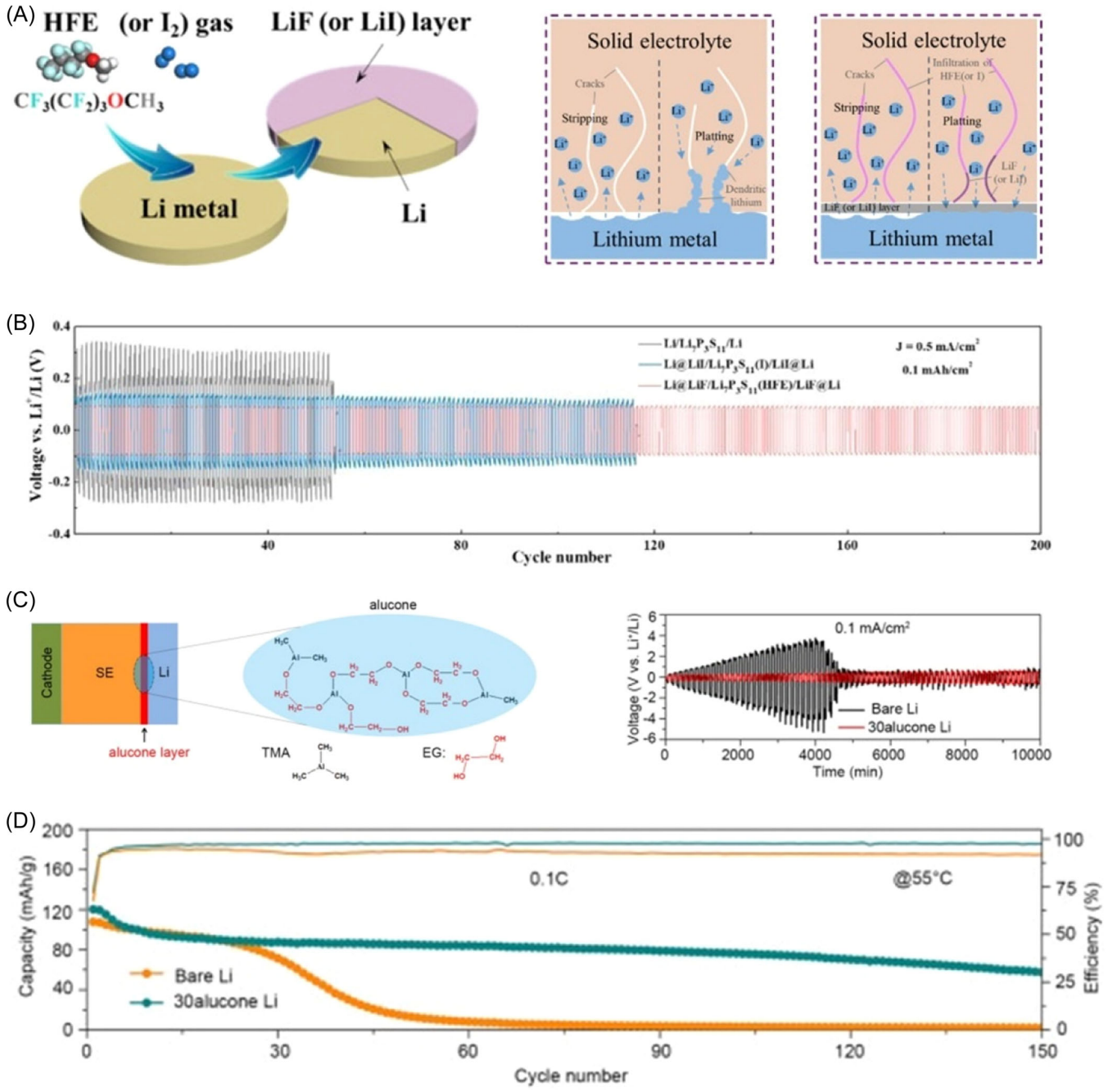

FIGURE 12 (A) Diagram demonstrating the LiF/LiI coating process on the Li metal surface as well as the behavior of Li stripping and plating when Li is bare and when LiF or LiI is coated Li with HFE or iodine infiltrated electrolyte. (B) Symmetrical cells at current densities of 0.5 mA cm^{-2}: Li@LiI/LPS(I)/LiI@Li (blue) and Li@LiF/LPS (HFE)/LiF@Li (red). (A and B) Reproduced with permission Xu et al.[69] Copyright 2018, Elsevier. (C) The configuration of the solid-state lithium metal battery (SSLMB) and chemical composition of alucone layer. (D) Cycle performance at 55°C of $LiCoO_2$-based SSLMBs. (C and D) Reproduced with permission Wang et al.[70] Copyright 2018, Elsevier.

remaining permanently stable. Janek's group was the first to discover that OLE reacts with $Li_{1+x}Al_xGe_{2-x}(PO_4)_3$ to form a solid–liquid electrolyte interphase (SLEI), causing an enlargement in interface impedance (Figure 15A,B).[96] Subsequently, Bruce et al. also found harmful SLEI in the LLZO system.[97] Figure 15C shows that the resistance and capacitance change over time, which indicates that the SSE/OLE interface is unstable and changing. Notably, resistance increased by ~22%, while capacitance decreased by ~23% during the same period. These are because the thickness of the ion conductive layer generated by the SSE surface side reaction increases with time, and the resistance and capacitance are directly proportional/inversely proportional

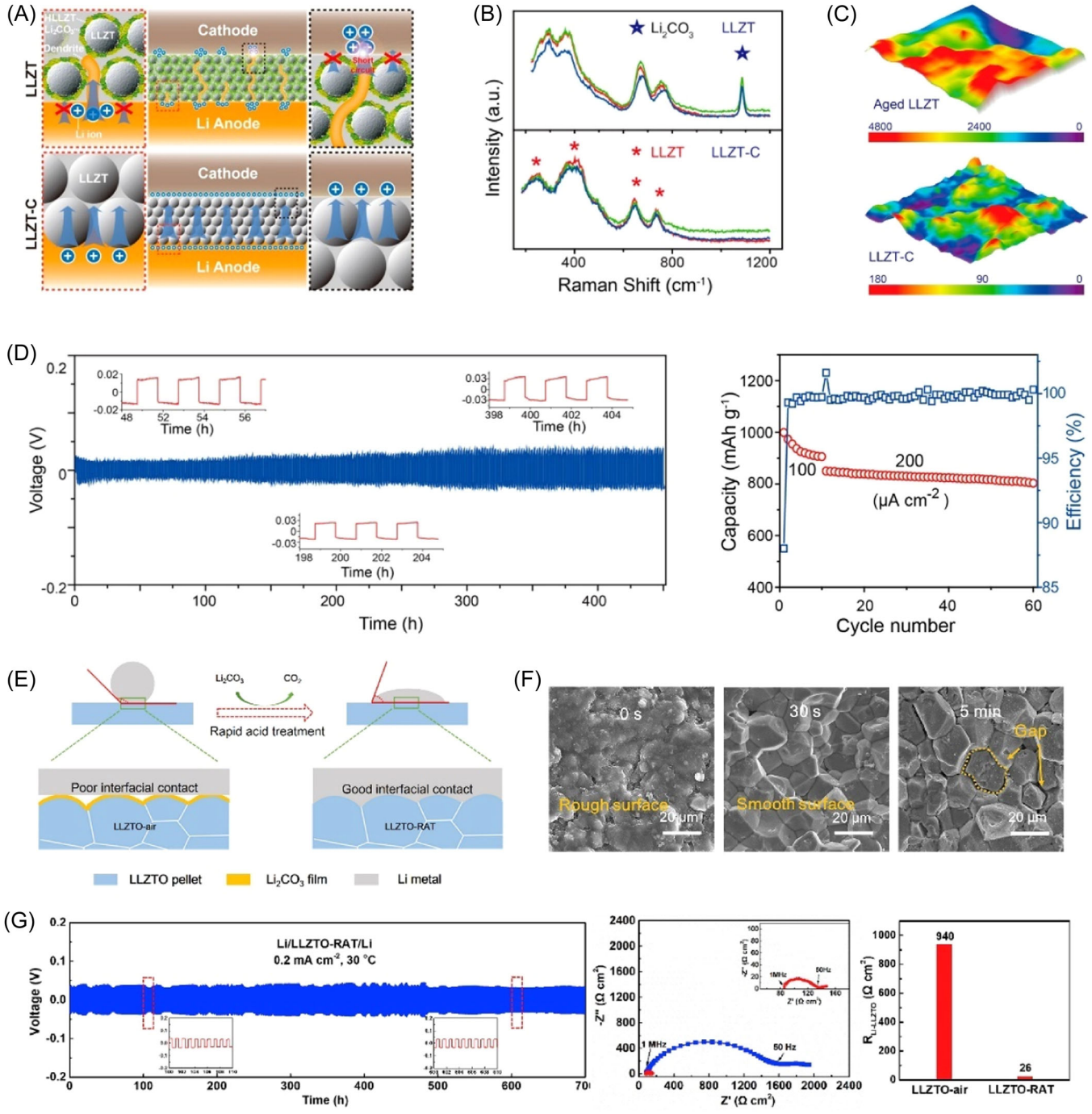

FIGURE 13 (A) Li-metal battery schematic featuring garnet LLZT and LLZT-C. (B) Comparison of LLZT and LLZT-C Raman spectra. (C) Raman mapping of LLZT and LLZT-C shows that LLZT has a thick layer of Li_2CO_3 on its surface, whereas LLZT that has been carbon treated does not have any Li_2CO_3. (D) At 65°C, the Li/LLZT-C/Li cell exhibits charge/discharge voltage profiles of 100 μA cm^{-2}, as well as capacity retention and cycling efficiency. (A–D) Reproduced with permission Li et al.[8] Copyright 2018, American Chemical Society. (E) Diagrammatic representation of the interface between Li and LLZTO before and after fast acid treatment. (F) The top-view scanning electron microscope images of aged LLZTO (LLZTO-air) and LLZTO after acid treatment (30 s, 5 min). (G) Li symmetric cells were electrochemically characterized at 30°C using samples of LLZTO-air and LLZTO samples that had undergone rapid acid treatment (LLZTO-RAT). The enlarged impedance curve of the LLZTO-RAT cell is displayed in the inset. (E–G) Reproduced with permission Huo et al.[92] Copyright 2019, Elsevier.

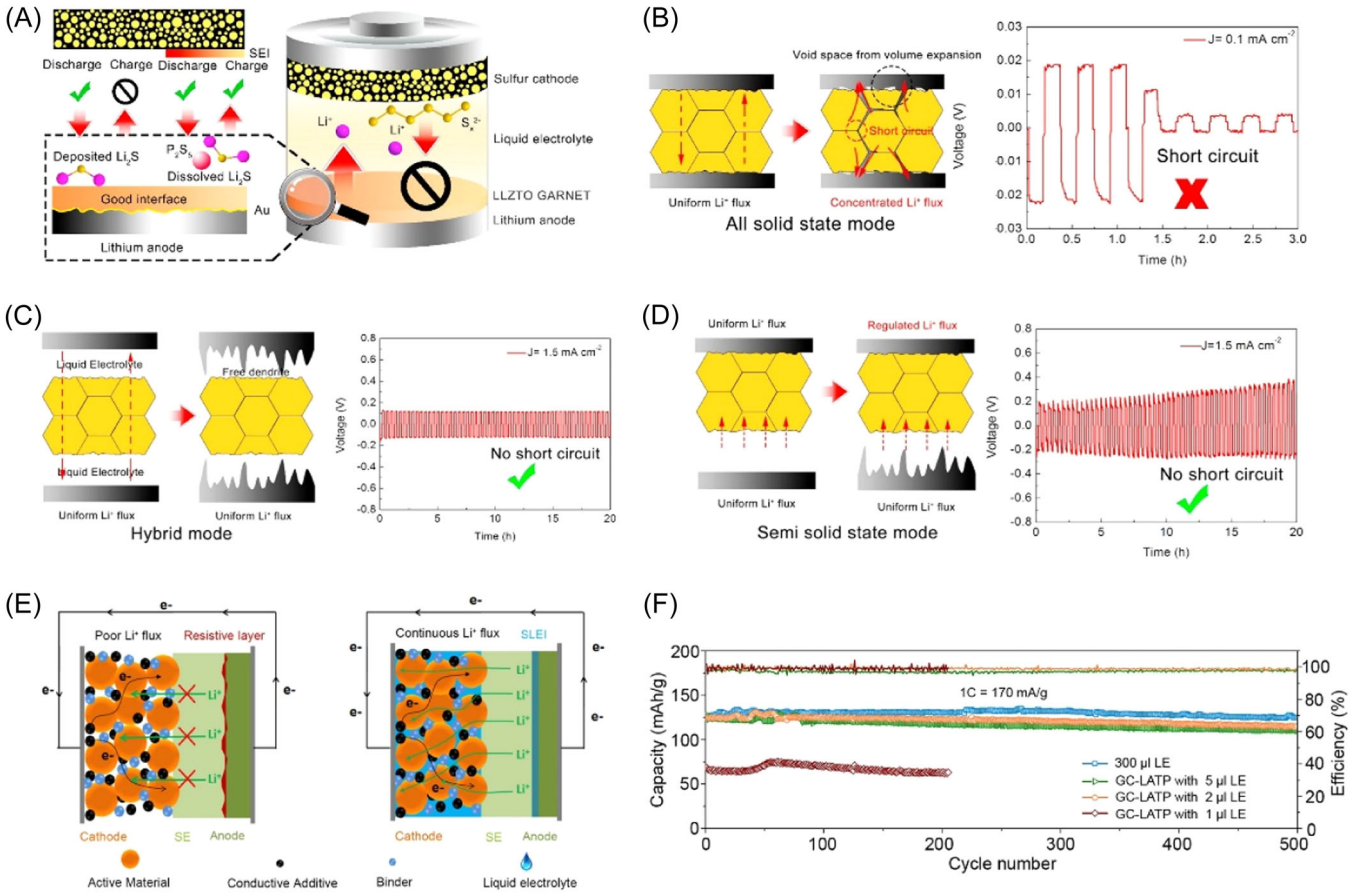

FIGURE 14 (A) Li-LLZTO-S battery schematic with corresponding mechanism and dual interphase modification. Diagrammatic representation of the Li-ion shuttle operating in four modes: (B) hybrid mode; (C) all-solid mode; (D) semisolid-state mode; and associated Li symmetric or semisymmetric cell. (A–D) Reproduced with permission Lu et al.[93] Copyright 2018, Elsevier. (E) Li^+ ion flux schematic diagram in three dimensions. (F) The sustained cycling performance of quasi-solid-state Li-ion batteries based on $LiFePO_4$ and using a glass-ceramic (GC)-LATP/LE hybrid electrolyte with a measured volume of organic liquid electrolyte at a current density of 1 C. (E and F) Reproduced with permission Wang et al.[95] Copyright 2018, Elsevier.

to the layer thickness, namely: $R \propto \rho l/A$ and $C \propto \varepsilon A/l$, where ρ is the resistivity and ε is electrical constant; A is the area of the layer and l is the thickness. For the sake of suppressing the formation of SLEI, Xu et al. added n-BuLi ultra-base to the organic electrolyte and adopted Lewis base to discourage the decomposition of OLE (Figure 15D).[98] The Raman spectroscopy clearly displays that LLZT exhibits Li_2CO_3 vibrational peaks at 156, 192, and 1090 cm^{-1} after being infiltrated by OLE. On the contrary, the Li_2CO_3 peaks disappear for the LLZT contacting with OLE adding n-BuLi (Figure 15E). Concurrently, highly protonated n-BuLi will prevent the exchange of Li^+/H^+, thereby avoiding the formation of SLEI and reducing the interface impedance from 1056 to 478 Ω cm^2 (Figure 15F). Another type is to replace the solvent system of traditional electrolytes with a new type of refractory liquid electrolyte to ensure the safety of the battery. Zhang and his colleagues incorporated 1-butyl-1-methylpyrrolidinium bis(trifluoromethylsulfonyl) imide (BMP-TFSI) ionic liquid into LLZO powder and formed a soft continuous coating at the surface interface of the composite electrolyte, as shown in Figure 15G.[99] This layer not only optimizes the interface contact mode, turning the point contact of the solid–solid interface into the surface contact of the solid–liquid, but also facilitates the uniform deposition of Li^+ at the interface on account of the preeminent Li conductivity of the ionic liquid, thus suppressing the formation of dendrites (Figure 15H).

5 | SUMMARY AND OUTLOOK

This review delves into the growth model of Li dendrites through the ion concentration gradient in SSE, the morphological characteristics of dendrites, and the nonuniform distribution of internal compressive stress. Furthermore, we highlight targeted solutions proposed by researchers in recent years to address these issues.

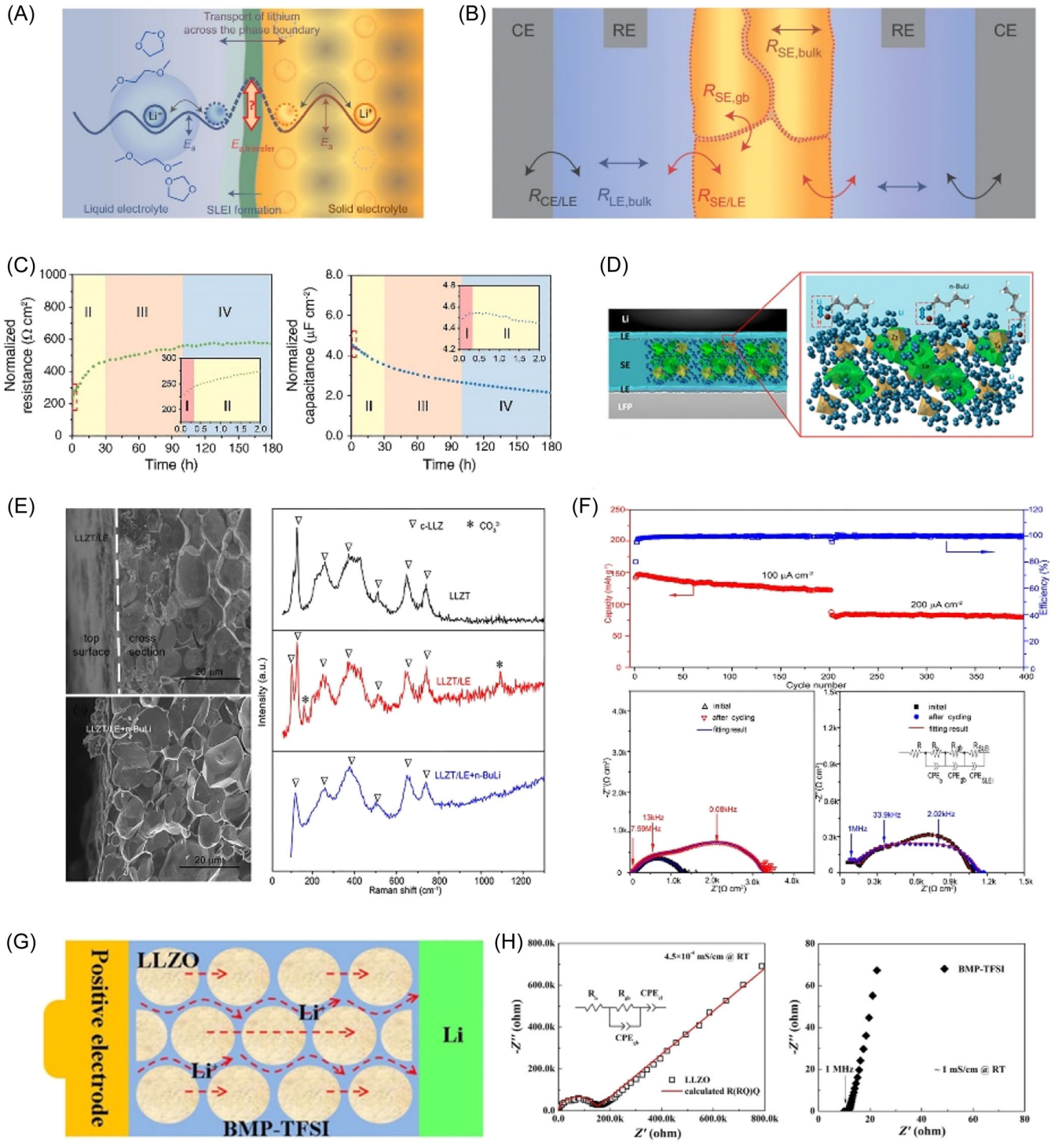

FIGURE 15 Diagrams showing the contributions of resistance and ion transport in cells with solid–liquid phase boundaries: (A) Transport of ions between liquid and solid electrolytes across their phase boundaries; (B) working principle of the 4 P set-up for electrochemical impedance spectroscopy (EIS) measurements on the organic liquid electrolyte (OLE)/solid-state electrolyte (SSE)/OLE cell. (A and B) Reproduced with permission Busche et al.[96] Copyright 2016, Springer Nature. (C) EIS measured the electrochemical impedance behavior of the LLZTO/LP30 interface with respect to time: interfacial resistance ($R_{SE/OLE}$) with respect to time (right); interfacial capacitance ($C_{SE/LE}$) with respect to time (left). Reproduced under terms of the CC-BY license Liu et al.[97] Copyright 2020, Elsevier. (D) Schematics showing how n-BuLi stabilizes the SSE/OLE interface. (E) Raman spectra and scanning electron microscope picture of LLZT as synthesized and LLZT after soaking in OLE containing/uncontaining n-BuLi. (F) Electrochemical characterization of the $LiFePO_4$/Li cell using hybrid electrolyte. (D–F) Reproduced with permission Xu et al.[98] Copyright 2017, American Chemical Society. (G) Diagrammatic representation of the 1-butyl-1-methylpyrrolidinium bis(trifluoromethylsulfonyl) imide (BMP-TFSI) coating layer's function. (H) Impedance spectra measured for pristine LLZO, BMP-TFSI. (G and H) Reproduced with permission Zhang et al.[99] Copyright 2018, Wiley.

Specifically: (i) Enhancing the ion conductivity/electronic insulation of SSE to improve Li-ion migration at the interface; (ii) Designing SSEs to immobilize anions through covalent bonding; (iii) Leveraging the high interface energy of the electrode contact surface to effectively block electron transfer; (iv) Introducing OLEs at the interface to transform the point contact of the solid–solid interface into solid–liquid surface contact.

Despite the remarkable progress in SSLMB research, several challenges persist. The future development of high-specific-energy SSLMBs should focus on the following aspects:

(1) Following the irregular growth model of Li metal, the extensive ion field, electric field, and pressure field within batteries can directly result in uneven Li deposition problems. However, various physical fields interact during the actual process, and it is imperative to establish more reasonable and practical multiphysical field coupling models. These models should enhance the regulation of Li-ion distribution and transport processes, along with influencing the growth mode of Li.
(2) Given the challenges posed by uncontrollable dendrites and poor interface stability, it is imperative to enhance the interface stability by designing the interface between the SSE and solid electrode. The synergistic interplay of interface components and structure critically influences the transport of Li ions and the deposition of Li. Typically, inorganic components offer a high mechanical modulus and superior ion conductivity, while organic components contribute to the toughness and pressure adaptability of the interface layer. However, actual interface layers often consist of multiple inorganic and organic components. A more in-depth and meticulous discussion of the interaction and compatibility between these diverse components is essential to guide a more rational design of the interface layer.
(3) Despite the considerable advantages of SSEs in terms of conductivity and electrochemical window, their power density is restricted by interface resistance and stability issues with both cathode and anode. Notably, the utilization of thicker SSEs in current practices tends to diminish the energy density of the overall battery. Consequently, the future direction involves the inevitable modification of SSEs to enhance the safety performance and energy density of batteries. This modification entails the addition of functional fillers to improve ion migration number and conductivity, the introduction of plasticizers to boost conductivity and facilitate interface wetting, and the development of high-voltage SSEs to align with high-voltage cathode materials.
(4) In addition, the electrochemical window is an important parameter for the working stability of SSEs, and its characterization is limited to experimental characterization and thermodynamic analysis and the electrochemical window of thermodynamic calculations is quite different from the electrochemical window of experimental characterization. The physical mechanism is not yet clear. It is also unclear how the doping ion concentration affects Li-ion transport and dendrite growth in the garnet phase LLZO system and the NASICON-type SSE system. Therefore, based on the above scientific issues, it is necessary to combine theoretical calculations (including first-principles calculations, molecular dynamics simulations, quantum chemical calculations, and electrochemical thermodynamics) and experimental research (including electronic structure analysis, fine characterization of electrode structure, and electrochemical performance testing) to study the electrochemical stability window of SSEs and the inherent coordinated mechanisms of Li-ion migration kinetics. Further screening of high-performance electrolyte materials is achieved through the dual optimization of electrochemical window composition and ion conductivity regulation.
(5) Enhanced characterization tools are imperative due to the intricate internal environment of SSEs, surpassing the complexity of OLEs, and the synergistic mechanics-chemistry-electricity working environment. The opacity of SSEs poses a challenge to traditional material characterization techniques, hindering a profound analysis of SSLMB failure mechanisms under operational conditions. To address this, researchers should progressively employ advanced in-situ characterization techniques for accurate real-time observation of the Li metal failure process in batteries and multiscale visualization of SSLMB failures. Techniques such as in-situ dual-beam electron microscopy (FIB-SEM), in-situ x-ray computed tomography, in-situ electron diffraction, in-situ neutron diffraction, and in-situ x-ray absorption near edge structure spectroscopy are essential. These methods facilitate cross-scale characterization and imaging, spanning from the centimeter to picometer level, allowing analysis of subtle chemical environmental changes, including elemental valence states of materials. Additionally, they effectively unveil the three-dimensional dynamic structure inside SSLMBs through sophisticated three-dimensional reconstruction techniques.
(6) Currently, alongside the analysis of interface performance through imaging technology, micro-area scanning electrochemical workstations should be employed to scrutinize interface reactions at sizes

ranging from several micrometers to even smaller scales. This approach aims to deepen our understanding of interface reaction mechanisms and facilitate the optimization and regulation of battery interface behavior.

ACKNOWLEDGMENTS

This work was supported financially by the Natural Sciences and Engineering Research Council of Canada (NSERC), Centre Québécois sur les Materiaux Fonctionnels (CQMF), the Canada Foundation for Innovation (CFI), Institut National de la Recherche Scientifique (INRS), and École de Technologie Supérieure (ÉTS). Dr. G. Zhang thanks for the support from the Marcelle-Gauvreau Engineering Research Chair program.

CONFLICT OF INTEREST STATEMENT

The authors declare no conflict of interest.

ORCID

Shuhui Sun https://orcid.org/0000-0002-0508-2944
Gaixia Zhang http://orcid.org/0000-0002-5340-8961

REFERENCES

1. Wu Z, Li XH, Zheng C, et al. Interfaces in sulfide solid electrolyte-based all-solid-state lithium batteries: characterization, mechanism and strategy. *Electrochem Energy R*. 2023;6(10).
2. Zhang S, Ma J, Dong S, Cui G. Designing all-solid-state batteries by theoretical computation: a review. *Electrochem Energy Rev*. 2023;6(1):4.
3. Cheng XB, Zhang R, Zhao CZ, Zhang Q. Toward safe lithium metal anode in rechargeable batteries: a review. *Chem Rev*. 2017;117(15):10403-10473.
4. Manthiram A, Yu X, Wang S. Lithium battery chemistries enabled by solid-state electrolytes. *Nat Rev Mater*. 2017;2(4):16103.
5. Yoon K, Lee S, Oh K, Kang K. Challenges and strategies towards practically feasible solid-state lithium metal batteries. *Adv Mater*. 2022;34(4):2104666.
6. Monroe C, Newman J. The impact of elastic deformation on deposition kinetics at lithium/polymer interfaces. *J Electrochem Soc*. 2005;152(2):A396-A404.
7. Liu Q, Chen Q, Tang Y, Cheng HM. Interfacial modification, electrode/solid-electrolyte engineering, and monolithic construction of solid-state batteries. *Electrochem Energy Rev*. 2023;6(1):15.
8. Li Y, Chen X, Dolocan A, et al. Garnet electrolyte with an ultralow interfacial resistance for Li-Metal batteries. *J Am Chem Soc*. 2018;140(20):6448-6455.
9. Cai M, Lu Y, Su J, et al. In situ lithiophilic layer from H/Li exchange on garnet surface for the stable lithium-solid electrolyte interface. *ACS Appl Mater Interfaces*. 2019;11(38):35030-35038.
10. Krauskopf T, Hartmann H, Zeier WG, Janek J. Toward a fundamental understanding of the lithium metal anode in solid-state batteries—an electrochemo-mechanical study on the Garnet-type solid electrolyte $Li_{6.25}Al_{0.25}La_3Zr_2O_{12}$. *ACS Appl Mater Interfaces*. 2019;11(15):14463-14477.
11. Wang MJ, Choudhury R, Sakamoto J. Characterizing the Li-solid-electrolyte interface dynamics as a function of stack pressure and current density. *Joule*. 2019;3(9):2165-2178.
12. Xie D, Chen S, Zhang Z, et al. High ion conductive Sb_2O_5-doped β-Li_3PS_4 with excellent stability against Li for all-solid-state lithium batteries. *J Power Sources*. 2018;389:140-147.
13. Yang C, Xie H, Ping W, et al. An electron/ion dual-conductive alloy framework for high-rate and high-capacity solid-state lithium-metal batteries. *Adv Mater*. 2019;31(3):1804815.
14. Duan J, Wu W, Nolan AM, et al. Lithium-graphite paste: an interface compatible anode for solid-state batteries. *Adv Mater*. 2019;31(10):1807243.
15. Li Y, Xu B, Xu H, et al. Hybrid polymer/garnet electrolyte with a small interfacial resistance for Lithium-ion batteries. *Angew Chem Int Ed*. 2017;56(3):753-756.
16. Mo Y, Ong SP, Ceder G. First principles study of the Li10GeP2S12Lithium super ionic conductor material. *Chem Mater*. 2012;24(1):15-17.
17. Zhao Q, Stalin S, Zhao C-Z, Archer LA. Designing solid-state electrolytes for safe, energy-dense batteries. *Nat Rev Mater*. 2020;5(3):229-252.
18. Li B, Chao Y, Li M, et al. A review of solid electrolyte interphase (SEI) and dendrite formation in lithium batteries. *Electrochem Energy Rev*. 2023;6(1):7.
19. Sun C, Ruan Y, Zha W, Li W, Cai M, Wen Z. Recent advances in anodic interface engineering for solid-state lithium-metal batteries. *Mater Horiz*. 2020;7(7):1667-1696.
20. Sharafi A, Kazyak E, Davis AL, et al. Surface chemistry mechanism of ultra-low interfacial resistance in the solid-state electrolyte $Li_7La_3Zr_2O_{12}$. *Chem Mater*. 2017;29(18):7961-7968.
21. Zheng H, Wu S, Tian R, et al. Intrinsic lithiophilicity of Li-garnet electrolytes enabling high-rate lithium cycling. *Adv Funct Mater*. 2020;30(6):7961-7968.
22. Cheng L, Crumlin EJ, Chen W, et al. The origin of high electrolyte-electrode interfacial resistances in lithium cells containing garnet type solid electrolytes. *Phys Chem Chem Phys*. 2014;16(34):18294-18300.
23. Liu C, Rui K, Shen C, Badding ME, Zhang G, Wen Z. Reversible ion exchange and structural stability of garnet-type Nb-doped $Li_7La_3Zr_2O_{12}$ in water for applications in lithium batteries. *J Power Sources*. 2015;282:286-293.
24. Krauskopf T, Dippel R, Hartmann H, et al. Lithium-metal growth kinetics on LLZO garnet-type solid electrolytes. *Joule*. 2019;3(8):2030-2049.
25. Zhang L, Yang T, Du C, et al. Lithium whisker growth and stress generation in an in situ atomic force microscope-environmental transmission electron microscope set-up. *Nat Nanotechnol*. 2020;15(2):94-98.
26. Aguesse F, Manalastas W, Buannic L, et al. Investigating the dendritic growth during full cell cycling of garnet electrolyte in direct contact with Li metal. *ACS Appl Mater Interfaces*. 2017;9(4):3808-3816.
27. Ren Y, Shen Y, Lin Y, Nan CW. Direct observation of lithium dendrites inside garnet-type lithium-ion solid electrolyte. *Electrochem Commun*. 2015;57:27-30.
28. Ebner M, Marone F, Stampanoni M, Wood V. Visualization and quantification of electrochemical and mechanical degradation in Li ion batteries. *Science*. 2013;342(6159):716-720.

29. Wang B, Li W, Wu T, Guo J, Wen Z. Self-template construction of mesoporous silicon submicrocube anode for advanced lithium ion batteries. *Energy Storage Mater*. 2018;15:139-147.
30. Peng P, Wen Z, Liu Y, Jin J. Improvement of lithium storage performance of Sn-alloy anode materials by a polypyrrole protective layer. *J Power Sources*. 2015;274:1100-1106.
31. Li H, Yamaguchi T, Matsumoto S, et al. Circumventing huge volume strain in alloy anodes of lithium batteries. *Nat Commun*. 2020;11(1):1584.
32. Agyeman DA, Song K, Lee GH, Park M, Kang YM. Carbon-coated si nanoparticles anchored between reduced graphene oxides as an extremely reversible anode material for high energy-density Li-ion battery. *Adv Energy Mater*. 2016;6(20):1600904.
33. Schweidler S, de Biasi L, Schiele A, Hartmann P, Brezesinski T, Janek J. Volume changes of graphite anodes revisited: a combined operando X-ray diffraction and in situ pressure analysis study. *J Phys Chem C*. 2018;122(16):8829-8835.
34. Haetge J, Hartmann P, Brezesinski K, Janek J, Brezesinski T. Ordered large-pore mesoporous $Li_4Ti_5O_{12}$ spinel thin film electrodes with nanocrystalline framework for high rate rechargeable lithium batteries: relationships among charge storage, electrical conductivity, and nanoscale structure. *Chem Mater*. 2011;23(19):4384-4393.
35. Huang S, Wen Z, Zhu X, Gu Z. Preparation and electrochemical performance of Ag doped $Li_4Ti_5O_{12}$. *Electrochem Commun*. 2004;6(11):1093-1097.
36. Wen Z, Gu Z, Huang S, Yang J, Lin Z, Yamamoto O. Research on spray-dried lithium titanate as electrode materials for lithium ion batteries. *J Power Sources*. 2005;146(1-2):670-673.
37. Cheng XB, Zhang R, Zhao CZ, Wei F, Zhang JG, Zhang Q. A review of solid electrolyte interphases on lithium metal anode. *Adv Sci*. 2016;3(3):1500213.
38. Wang P, Qu W, Song WL, Chen H, Chen R, Fang D. Electro-chemo-mechanical issues at the interfaces in solid-state lithium metal batteries. *Adv Funct Mater*. 2019;29(27):1900950.
39. Hovington P, Lagacé M, Guerfi A, et al. New lithium metal polymer solid state battery for an ultrahigh energy: nano C-$LiFePO_4$ versus nano $Li_{1.2}V_3O_8$. *Nano Lett*. 2015;15(4):2671-2678.
40. Koerver R, Zhang WB, de Biasi L, et al. Chemo-mechanical expansion of lithium electrode materials—on the route to mechanically optimized all-solid-state batteries. *Energy Environ Sci*. 2018;11(8):2142-2158.
41. Cheng EJ, Sharafi A, Sakamoto J. Intergranular Li metal propagation through polycrystalline $Li_{6.25}Al_{0.25}La_3Zr_2O_{12}$ ceramic electrolyte. *Electrochim Acta*. 2017;223:85-91.
42. Zhang X, Wang A, Liu X, Luo J. Dendrites in lithium metal anodes: suppression, regulation, and elimination. *Acc Chem Res*. 2019;52(11):3223-3232.
43. Chazalviel JN. Electrochemical aspects of the generation of ramified metallic electrodeposits. *Phys Rev A*. 1990;42(12):7355-7367.
44. Zheng JM, Wu XB, Yang Y. A comparison of preparation method on the electrochemical performance of cathode material $Li[Li_{0.2}Mn_{0.54}Ni_{0.13}Co_{0.13}]O_2$ for lithium ion battery. *Electrochim Acta*. 2011;56(8):3071-3078.
45. Wang X, Zeng W, Hong L, et al. Stress-driven lithium dendrite growth mechanism and dendrite mitigation by electroplating on soft substrates. *Nat Energy*. 2018;3(3):227-235.
46. Ely DR, García RE. Heterogeneous nucleation and growth of lithium electrodeposits on negative electrodes. *J Electrochem Soc*. 2013;160(4):A662-A668.
47. Xiao J. How lithium dendrites form in liquid batteries. *Science*. 2019;366(6464):426-427.
48. Sand HJS. On the concentration at the electrodes in a solution, with special reference to the liberation of hydrogen by electrolysis of a mixture of copper sulphate and sulphuric acid. *Proc Phys Soc*. 1899;17(1):496-534.
49. Chang HJ, Ilott AJ, Trease NM, Mohammadi M, Jerschow A, Grey CP. Correlating microstructural lithium metal growth with electrolyte salt depletion in lithium batteries Using 7Li MRI. *J Am Chem Soc*. 2015;137(48):15209-15216.
50. Brissot C, Rosso M, Chazalviel JN, Lascaud S. In situ concentration cartography in the neighborhood of dendrites growing in lithium/polymer-electrolyte/lithium cells. *J Electrochem Soc*. 1999;146(12):4393-4400.
51. Li W, Yao H, Yan K, et al. The synergetic effect of lithium polysulfide and lithium nitrate to prevent lithium dendrite growth. *Nat Commun*. 2015;6:7436.
52. Qian J, Henderson WA, Xu W, et al. High rate and stable cycling of lithium metal anode. *Nat Commun*. 2015;6:1155.
53. Cao R, Chen J, Han KS, et al. Effect of the anion activity on the stability of Li metal anodes in lithium-sulfur batteries. *Adv Funct Mater*. 2016;26(18):3059-3066.
54. Bazant MZ, Choi J, Davidovitch B. Dynamics of conformal maps for a class of non-Laplacian growth phenomena. *Phys Rev Lett*. 2003;91(4):045503.
55. Bai P, Li J, Brushett FR, Bazant MZ. Transition of lithium growth mechanisms in liquid electrolytes. *Energy Environ Sci*. 2016;9(10):3221-3229.
56. Monroe C, Newman J. Dendrite growth in lithium/polymer systems. *J Electrochem Soc*. 2003;150(10):A1377-A1384.
57. Krauskopf T, Richter FH, Zeier WG, Janek J. Physicochemical concepts of the lithium metal anode in solid-state batteries. *Chem Rev*. 2020;120(15):7745-7794.
58. Chason E, Jadhav N, Pei F, Buchovecky E, Bower A. Growth of whiskers from Sn surfaces: driving forces and growth mechanisms. *Prog Surf Sci*. 2013;88(2):103-131.
59. Harry KJ, Hallinan DT, Parkinson DY, MacDowell AA, Balsara NP. Detection of subsurface structures underneath dendrites formed on cycled lithium metal electrodes. *Nat Mater*. 2014;13(1):69-73.
60. Kushima A, So KP, Su C, et al. Liquid cell transmission electron microscopy observation of lithium metal growth and dissolution: root growth, dead lithium and lithium flotsams. *Nano Energy*. 2017;32:271-279.
61. Jana A, Woo SI, Vikrant KSN, García RE. Electrochemomechanics of lithium dendrite growth. *Energy Environ Sci*. 2019;12(12):3595-3607.
62. Suyama M, Kato A, Sakuda A, Hayashi A, Tatsumisago M. Lithium dissolution/deposition behavior with Li_3PS_4-LiI electrolyte for all-solid-state batteries operating at high temperatures. *Electrochim Acta*. 2018;286:158-162.
63. Han F, Yue J, Zhu X, Wang C. Suppressing Li dendrite formation in Li_2S-P_2S_5 solid electrolyte by LiI incorporation. *Adv Energy Mater*. 2018;8(18):1703644.

64. Zhang H, Li C, Piszcz M, et al. Single lithium-ion conducting solid polymer electrolytes: advances and perspectives. *Chem Soc Rev*. 2017;46(3):797-815.
65. Cao C, Li Y, Feng Y, Peng C, Li Z, Feng W. A solid-state single-ion polymer electrolyte with ultrahigh ionic conductivity for dendrite-free lithium metal batteries. *Energy Storage Mater*. 2019;19:401-407.
66. Tikekar MD, Archer LA, Koch DL. Stabilizing electrodeposition in elastic solid electrolytes containing immobilized anions. *Sci Adv*. 2016;2(7):e1600320.
67. Ye L, Li X. A dynamic stability design strategy for lithium metal solid state batteries. *Nature*. 2021;593(7858):218-222.
68. Liang JY, Zeng XX, Zhang XD, et al. Engineering Janus interfaces of ceramic electrolyte via distinct functional polymers for stable high-voltage Li-metal batteries. *J Am Chem Soc*. 2019;141(23):9165-9169.
69. Xu R, Han F, Ji X, Fan X, Tu J, Wang C. Interface engineering of sulfide electrolytes for all-solid-state lithium batteries. *Nano Energy*. 2018;53:958-966.
70. Wang C, Zhao Y, Sun Q, et al. Stabilizing interface between $Li_{10}SnP_2S_{12}$ and Li metal by molecular layer deposition. *Nano Energy*. 2018;53:168-174.
71. Han X, Gong Y, Fu K, et al. Negating interfacial impedance in garnet-based solid-state Li metal batteries. *Nat Mater*. 2017;16(5):572-579.
72. Wang C, Gong Y, Liu B, et al. Conformal, nanoscale ZnO surface modification of garnet-based solid-state electrolyte for lithium metal anodes. *Nano Lett*. 2017;17(1):565-571.
73. He M, Cui Z, Chen C, Li Y, Guo X. Formation of self-limited, stable and conductive interfaces between garnet electrolytes and lithium anodes for reversible lithium cycling in solid-state batteries. *J Mater Chem A*. 2018;6(24):11463-11470.
74. Tsai CL, Roddatis V, Chandran CV, et al. $Li_7La_3Zr_2O_{12}$ interface modification for Li dendrite prevention. *Acs Appl Mater Inter*, 20168(16):10617-10626.
75. Wakasugi J, Munakata H, Kanamura K. Effect of gold layer on interface resistance between lithium metal anode and $Li_{6.25}Al_{0.25}La_3Zr_2O_{12}$ solid electrolyte. *J Electrochem Soc*. 2017;164(6):A1022-A1025.
76. Zhao N, Fang R, He MH, et al. Cycle stability of lithium/garnet/lithium cells with different intermediate layers. *Rare Met*. 2018;37(6):473-479.
77. Fu K, Gong Y, Fu Z, et al. Transient behavior of the metal interface in lithium metal-garnet batteries. *Angew Chem Int Ed*. 2017;56(47):14942-14947.
78. Xiang X, Cao S, Chen F, Shen Q, Zhang L. Communication-Li/$Li_7La_3Zr_2O_{12}$ interfacial modification by constructing a layer of Cu-Li alloy. *J Electrochem Soc*. 2019;166(13):A3028-A3030.
79. Lou J, Wang G, Xia Y, et al. Achieving efficient and stable interface between metallic lithium and garnet-type solid electrolyte through a thin indium tin oxide interlayer. *J Power Sources*. 2020;448:227440.
80. Pervez SA, Ganjeh-Anzabi P, Farooq U, Trifkovic M, Roberts EPL, Thangadurai V. Fabrication of a dendrite-free all solid-state Li metal battery via polymer composite/garnet/polymer composite layered electrolyte. *Adv Mater Interfaces*. 2019;6(11):1900186.
81. Fu JM, Yu PF, Zhang N, et al. In situ formation of a bifunctional interlayer enabled by a conversion reaction to initiatively prevent lithium dendrites in a garnet solid electrolyte. *Energy Environ Sci*. 2019;12(4):1404-1412.
82. Meng J, Zhang Y, Zhou X, Lei M, Li C. Li_2CO_3-affiliative mechanism for air-accessible interface engineering of garnet electrolyte via facile liquid metal painting. *Nat Commun*. 2020;11(1):3716.
83. Zhong YR, Xie YJ, Hwang S, et al. A highly efficient all-solid-state lithium/electrolyte interface induced by an energetic reaction. *Angew Chem Int Edit*. 2020;59(33):14003-14008.
84. Zhou C, Samson AJ, Hofstetter K, Thangadurai V. A surfactant-assisted strategy to tailor Li-ion charge transfer interfacial resistance for scalable all-solid-state Li batteries. *Sustain Energy Fuels*. 2018;2(10):2165-2170.
85. Zheng S, Fu Z, Dai D, Zhao W. Tuning the interface by a soldering method for high performance garnet-type solid-state Li metal battery. *Ceram Int*. 2019;45(9):11955-11962.
86. Gao J, Zhu J, Li X, et al. Rational design of mixed electronic-ionic conducting Ti-doping $Li_7La_3Zr_2O_{12}$ for lithium dendrites suppression. *Adv Funct Mater*. 2021;31(2):2001918.
87. Luo W, Gong Y, Zhu Y, et al. Reducing interfacial resistance between garnet-structured solid-state electrolyte and Li-metal anode by a germanium layer. *Adv Mater*. 2017;29(22):1606042.
88. Luo W, Gong Y, Zhu Y, et al. Transition from superlithiophobicity to superlithiophilicity of garnet solid-state electrolyte. *J Am Chem Soc*. 2016;138(37):12258-12262.
89. Wu JF, Pu BW, Wang D, et al. In situ formed shields enabling Li_2CO_3-free solid electrolytes: a new route to uncover the intrinsic lithiophilicity of garnet electrolytes for dendrite-free Li-metal batteries. *ACS Appl Mater Interfaces*. 2019;11(1):898-905.
90. Xu S, McOwen DW, Wang C, et al. Three-dimensional, solid-state mixed electron-ion conductive framework for lithium metal anode. *Nano Lett*. 2018;18(6):3926-3933.
91. Xu B, Li W, Duan H, et al. Li_3PO_4-added garnet-type $Li_{6.5}La_3Zr_{1.5}Ta_{0.5}O_{12}$ for Li-dendrite suppression. *J Power Sources*. 2017;354:68-73.
92. Huo H, Chen Y, Zhao N, et al. In-situ formed Li_2CO_3-free garnet/Li interface by rapid acid treatment for dendrite-free solid-state batteries. *Nano Energy*. 2019;61:119-125.
93. Lu Y, Huang X, Song Z, et al. Highly stable garnet solid electrolyte based Li-S battery with modified anodic and cathodic interfaces. *Energy Storage Mater*. 2018;15:282-290.
94. Huo H, Zhao N, Sun J, Du F, Li Y, Guo X. Composite electrolytes of polyethylene oxides/garnets interfacially wetted by ionic liquid for room-temperature solid-state lithium battery. *J Power Sources*. 2017;372:1-7.
95. Wang C, Sun Q, Liu Y, et al. Boosting the performance of lithium batteries with solid-liquid hybrid electrolytes: interfacial properties and effects of liquid electrolytes. *Nano Energy*. 2018;48:35-43.
96. Busche MR, Drossel T, Leichtweiss T, et al. Dynamic formation of a solid-liquid electrolyte interphase and its consequences for hybrid-battery concepts. *Nat Chem*. 2016;8(5):426-434.
97. Liu J, Gao X, Hartley GO, et al. The interface between $Li_{6.5}La_3Zr_{1.5}Ta_{0.5}O_{12}$ and liquid electrolyte. *Joule*. 2020;4(1):101-108.
98. Xu B, Duan H, Liu H, Wang A, Zhong S. Stabilization of garnet/liquid electrolyte interface using superbase additives

for hybrid li batteries. *ACS Appl Mater Interfaces*. 2017;9(25): 21077-21082.

99. Zhang Z, Zhang L, Liu Y, et al. Interface-engineered $Li_7La_3Zr_2O_{12}$-based garnet solid electrolytes with suppressed Li-dendrite formation and enhanced electrochemical performance. *ChemSusChem*. 2018;11(21):3774-3782.

AUTHOR BIOGRAPHIES

Huaihu Sun is currently a PhD candidate at the Institut National de la Recherche Scientifique (INRS), center for Energy, Materials, and Telecommunications, Canada. His research focuses on interface engineering for solid-state batteries.

Shuhui Sun is a Full Professor at the Institut National de la Recherche Scientifique (INRS), center for Energy, Materials, and Telecommunications, Canada. He is a Fellow of the Canadian Academy of Engineering (CAE), and a Member of the Royal Society of Canada (RSC College). His current research interests focus on multifunctional nanomaterials for energy conversion and storage applications, including H_2 fuel cells, metal-ion (Li, Na, Zn) batteries, lithium-metal batteries, metal-air batteries, solid-state batteries, and so on. He is also interested in nanostructured photo- and electro-catalysts for H_2 production, CO_2 reduction, and water treatment.

Gaixia Zhang is a Marcelle-Gauvreau Engineering Research Chair Professor at École de Technologie Supérieure (ÉTS), University of Quebec, Montréal, Canada. She received her PhD degree from Polytechnique Montréal and then continued her research at Western University and INRS, Canada. Her research interests focus on advanced materials (catalysts, electrodes, and electrolytes) for sustainable energy conversion and storage applications, including batteries, fuel cells, hydrogen production, and CO_2 reduction. She is also interested in interface and device engineering, as well as in-situ characterizations and theoretical simulations.

How to cite this article: Sun H, Celadon A, Cloutier SG, Al-Haddad K, Sun S, Zhang G. Lithium dendrites in all-solid-state batteries: from formation to suppression. *Battery Energy*. 2024;3:20230062. doi:10.1002/bte2.20230062